

ACIT5930
MASTER'S THESIS

in

**Applied Computer and Information
Technology (ACIT)**

June 2022

Biomedical Engineering

**Analysis of
Magnesium Implant - tissue Interface**

Anna Mathew

**Department of Mechanical Electrical and Chemical Engineering
Faculty of Technology, Art and Design**

OSLOMET

Preface

The work is part of the course ACIT5930 thesis phase3, which includes work from January 2021 to May 2022. It provides literature study, lab works, software-based analysis, and discussion. This work collaborates with a Ph.D. candidate of OsloMet, Hafiz Wajahat Hassan, who works for MSCA-ITN-ETN "MgSafe" under the Marie Skłodowska Curie grant agreement No 811226.

I want to express my sincere gratitude to my principal supervisor, professor Peyman Mirtaheri, for giving me this research opportunity and valuable guidance. His frequent meetings and discussions gave me constructive ideas, as they helped me proceed further when faced with difficulties. He used to give me new ways of looking at problems. His energy to help, enthusiasm to find new facts, and knowledge in biomedical engineering and data analysis are inspiring. I am grateful to him for being a motivator to try differently without fear. Even in the most challenging situations, he supports getting resources and facilities from OsloMet, obeying the pandemic guidelines.

I am grateful to Professor Olga Korostynska, my co-supervisor, for providing me with new platforms to work. Her promptness in replying to my concerns and service requests helped me digitally connect with OsloMet. She ensured that I got all lab facilities and software help. She helped and supported new opportunities to participate in the international platform, where we got recognized for our efforts. I am thankful for her continuous guidance to think in a product approach that gave me new insights to view the problem. She continuously motivates me to conquer new opportunities to help me grow as a promising researcher.

Professor Frank Westward from NTNU University, my co-supervisor, gave valuable tips that helped me uncover new research activities. Having physical meetings for discussion was not practical as the professor works in a different university. I wish to mention that he opened up broad areas to think, learn, and explore through the online discussions. His knowledge and exposure to NIR spectroscopy and data analysis software are inspiring. I am grateful for his discussions, research directions, and time.

I would also like to express my sincere gratitude to Ph.D. candidate Hafiz Wajahat Hassan, the backbone of my lab studies at OsloMet. He has good patience in explaining and showing me the lab facilities at OsloMet. His kindness in allowing me to be part of his research activities helped me generate substantial interest in my chosen area. His discussions helped clear my doubts and developed the confidence to try new research methods in the lab. Wajahat found time within his schedule to guide me. I am grateful that he supported gathering datasets used for the conference and *in vitro* experiments. I want to express my gratitude to the research team at the Institute of Clinical Physiology, CNR, San Cataldo Research Area, Italy, who were *in vivo* experiment team. I am also thankful to the MgSafe research group at OsloMet for providing facilities and data from different experiments, without which my thesis would be incomplete.

Professor Per Ola Rønning supported by providing chemistry lab facilities to prepare the gels used for the experiment. Engineer Tore Øfsdahl helped set up my laptop, the software Unscrambler remotely. Engineer Morten Ødegård helped me get the components needed for my electronics lab work. He even took the trouble to purchase components needed for my experiments. I am grateful to my friend Meera Joseph, working as a data scientist in Basefarm, for helping me with modeling ideas.

I thank my husband, Basil Boon K, for his patience and motivation to study in Norway. His unconditional love and support in handling my family's needs helped me finish my course requirements. I am grateful for the endless love and support of my twin boys, Jayden, and Jordon, who understand and encourage me to study. Finally, my infinite love and joy for my little daughter Janet make our lives refreshing.

Anna Mathew

Oslo, Norway

Date: 16 May 2022

Abstract

As people become old, there is a significant growth in osteoporosis-related fractures. Modern days require improvements in implants that are used in orthopedic interventions imperative. Biodegradable Magnesium (Mg) based implants were recently developed to replace non-degradable metallic implants. It is a viable and patient-friendly method for health care from patients' viewpoints. The Near-Infrared Spectroscopy (NIRS) area is in the range of 650-1100nm, which interacts with biological tissues is interesting in this regard.

The project is associated with MSCA-ITN Horizon 2020 (MgSafe), which focuses on magnesium-based implant experiments. The target is to collect the NIR spectrum using an optical probe to detect changes at the magnesium-implant tissue interface. The thesis covers the study that connects *in vitro* works (lab-based experiments) at OsloMet to support the *in vivo* (animal-based) experiments conducted by the MgSafe researcher's team in Italy. With the reduction in pandemic restriction, it was possible to gather data from rats, which was advantageous for a realistic exploratory study.

The *in vitro* experiment studies biodegradable and non-biodegradable implant disks in an artificially created medium. It identifies the trend that there is a possibility to group the optical data based on different days, which is helpful for the *in vivo* experiment. A primary challenge for *in vivo* experiment is the complexity of the interaction of magnesium implant near interface summed up with the issues due to light scattering in a biological medium. This thesis aims to study the feasibility of using the optical spectrum to understand the progress of implant surgery near the implant tissue interface. It performs a multivariate explanatory study using the developed optical probe and relates the *in vitro* experiments with the *in vivo* experiments. This work compares the optical information from healthy and unhealthy animals as unique case studies. The thesis covers observations and suggestions for future researchers in this area.

Keywords: Biodegradable implants, Magnesium implants, Biomarker, NIR spectroscopy, Optical probe, Multivariate analysis, Data analysis.

Table of Contents

Contents

Preface	1
Abstract	3
Table of Contents	4
List of Figure	6
List of Tables	9
1. Introduction	10
1.1 Problem Statement and Research Questions	11
1.2 Structure of Report.....	12
2. Literature review & methodology.....	13
2.1 Background	13
2.2 Methodology.....	16
2.2.1 Data collection approaches	17
2.2.2 Data analysis	17
3. <i>In vitro</i> lab experiments and their results.....	20
3.1 Experiment setup and data preprocessing	21
3.1.1 Procedure.....	21
3.1.2 Preprocessing of <i>In vitro</i> dataset	22
3.2 Observations of <i>In vitro</i> DMEM experiment.....	25
3.2.1 Trend observed from <i>in vitro</i> experiment.....	26
3.3 pH curve based <i>in vitro</i> experiment.....	27
3.4 A look into non-biodegradable titanium implant	29
4. Additional <i>In vitro</i> preparatory experiments	31
4.1 Probe Studies	31
4.2.1 Experiment 2: Dead tissue experiment and its results	33
4.2.2 Experiment 3: Gel Based Experiment and its results.....	36
5. <i>In vivo</i> experiment results.....	38
5.1 Research Ethics and overview of the dataset	38
5.2 Preprocessing and the pipeline for <i>in vivo</i> dataset.....	39
5.2 Principal component analysis (PCA) of <i>In vivo</i> Data	43
5.3 Additional details about the rats used in the Model studies.....	45
5.4 Wavelengths of significance.....	47

6. Discussions	52
6.1 The biomarker pH	52
6.1.1 What is pH?	53
6.2 Chemicals at the interface	54
6.3 Optical medium properties	55
6.4 <i>In vitro</i> Vs <i>In vivo</i>	56
6.4.1 <i>In vitro</i> DMEM experiment	56
6.4.2 <i>In vivo</i> experiments	57
6.4.3 Special case study from <i>in vivo</i> : Unhealthy and Died Rats	57
6.5 Strength and weakness of the model	59
7. Challenges & future scope	60
7.1 Timeline for thesis.....	60
7.2 Challenges Faced.....	61
7.2.1 Pandemic challenges.....	61
7.2.2 Concerns in the software platform	61
7.2.3 Issues related to a prediction based model	62
7.3 Future Directions for researchers	63
7.3.1 Data collection	63
7.3.2 Prediction model based on classification approach	64
7.3.3 Probe studies	67
7.4 Future scope.....	67
Conclusion.....	70
Reference List.....	71
Appendices.....	74
Appendix A: Additional Achievement	74
A1: Main author conference publication	74
A2: IEEE conference publication details (Co-author)	75
Appendix B: Python code snippets	76
Appendix C: Calibration procedure	78

List of Figure

<i>Figure 2. 1 Biocompatibility of biodegradable Mg-based orthopedic implants (Wang et al., 2020) *</i>	14
<i>Figure 2. 2 Ideal degradation pattern of the biodegradable fixators to support healing completion at the fracture site. (Wang et al., 2020) *</i>	15
<i>Figure 2. 3 Experimental arrangement for reflection-based measurement done In vitro liquid-based medium (a) Path of light in the medium (b) lab set up (c) Illustration of the light source and detector for transmission type of arrangement.....</i>	17
<i>Figure 2. 4 Reflection based measurement (a) Commercial probe (b) OsloMet probe (c) In vivo (animal Model) experiments have biological complexity due to the medium.....</i>	17
<i>Figure 2. 5 Flow chart for the methodology</i>	19
<i>Figure 3. 1 (a) pH meter at UiO (b) pH of a medium is alkaline if OH⁻ ions are more than H⁺ ions.....</i>	20
<i>Figure 3. 2 Flow chart for the data processing for the in vitro experiment</i>	22
<i>Figure 3. 3 Mg Alloy DMEM Data (a) Raw Data (b) scaled data</i>	23
<i>Figure 3. 4 Score plot for Mg Alloy implant material (PC1- PC2) (a) 3 D plot and (b) 2D plot</i>	24
<i>Figure 3. 5 PCA of data after removing outlier (10 samples taken on Day 5 from Sample 3). Still, we see that measurements from day five sample 1 influence PC1. It concludes that day 5 samples are inconsistent data in the group. There is a need for additional samples per category for future research.</i>	25
<i>Figure 3. 6 The trend on timepoint based on the complete Mg Alloy implant dataset.</i>	27
<i>Figure 3. 7 pH of the different mediums on different days. The plot is the average of three samples.....</i>	28
<i>Figure 3. 8 Titanium implant-based PCA</i>	29
<i>Figure 4. 1 OsloMet probe for reflection-based measurements from the surface.....</i>	32
<i>Figure 4. 2 Illustration of optical Probe and Data collection (Hassan, Mathew, et al., 2021)</i>	32
<i>Figure 4. 3 Probe used for experiment (a) commercial Probe manufactured by Avantes (b) OsloMet Probe</i>	33
<i>Figure 4. 4 Eleven different selected points</i>	34
<i>Figure 4. 5 Spectroscopic data plot (a) for varying thickness obtained from OsloMet probe (b)For varying thickness obtained from Avantes probe</i>	34
<i>Figure 4. 6 (a) PCA of post-mortem animal tissue Study of Avantes Probe Scatter plot from Unscrambler software (b) PCA study of OsloMet Probe, score plot from Unscrambler software.....</i>	35

<i>Figure 4. 7 Principal component analysis (PCA) for 6mm and 8mm source distance measurement of optical probe (blue dots are 6mm and yellow dots are 8mm).....</i>	<i>36</i>
<i>Figure 5. 1 Data collection for in vivo experiments.....</i>	<i>38</i>
<i>Figure 5. 2 Right and Left femur data points from all-day conditions for Mg Implant Rats (a) First two PCA (b) First 3 PCA. Left femur data have more outliers compared to right femur.</i>	<i>40</i>
<i>Figure 5. 3 Flow chart for the data analysis for the in vivo experiment</i>	<i>41</i>
<i>After repeated close analysis of filters and their application order, I observed trends similar to in vitro data in the PC1-PC2 plain that separates the optical data to different time points. Figure 5.3 shows the preprocessing of the in vivo data flow, which helped me see the trend. Unlike the DMEM in vitro data analysis pipeline, it uses two other preprocess approaches: a scatter technique known as standard normal variate or SNV and a derivative filter.....</i>	<i>41</i>
<i>Figure 5. 4 Raw in vivo data as obtained from the spectrometer for Mg alloy Right implant.....</i>	<i>42</i>
<i>Figure 5. 5 Preprocessed data by the end of step3 in the flowchart. It is the input for PCA analysis</i>	<i>43</i>
<i>Figure 5. 6 Explained Variance of PCA in figure 5.7.....</i>	<i>43</i>
<i>Figure 5. 7 PCA of MgAlloy implant-based optical data-based PCA of the right femur. The first two PCA plotted in the 2D plot</i>	<i>44</i>
<i>Figure 5. 8 PCA of MgAlloy implant-based optical data-based PCA of the right femur. The First 3 PCA components plotted in the 3D plot</i>	<i>44</i>
<i>Figure 5. 9 PCA concerning PC1 and PC2 based on different days.....</i>	<i>44</i>
<i>Figure 5. 10 Initial Orange-based observations.....</i>	<i>45</i>
<i>Figure 5. 11 PC1 -PC2 plot highlighting different timepoints where the unhealthy rats are in white with label..</i>	<i>47</i>
<i>Figure 5. 12 Loading plot and preprocessed optical data from the right femur of all rats having Mg implant ...</i>	<i>48</i>
<i>Figure 5. 13 Loading plot and preprocessed optical data from the right femur of healthy rats alone.....</i>	<i>48</i>
<i>Figure 5. 14 Derivative spectra of day 0</i>	<i>49</i>
<i>Figure 5. 15 Derivative spectra of day 3</i>	<i>50</i>
<i>Figure 5. 16 Derivative spectra of day 7</i>	<i>50</i>
<i>Figure 5. 17 Derivative spectra of day 14</i>	<i>51</i>
<i>Figure 6. 1 Variation in the presence of different chemicals near the interface.....</i>	<i>55</i>
<i>Figure 6. 2 Summary of Elements present in the Magnesium implant surface from in vitro experiments.</i>	<i>55</i>

The least prominent element is Zinc. The implant is an alloy having zinc in it. Its presence is unseen in the upcoming day. Figure 6.2 summarises the elements present on the magnesium alloy implant. (Zhang et al., 2009) in vivo studies mention P, C, Ca, O, and Mg in an in vivo Magnesium implant analysis. 55

Figure 6. 3 (A) Gas cavity size evolution throughout the implantation period; and (B) gas cavity size at different rat parts. (Deni Noviana a, 2016, p. 11). 56

Figure 7. 1 In vitro experiment based on PCA highlighting the samples of day 5 62

Figure 7. 2 (a) Binary classifier (b) Muti class Confusion Matrix: a general representation (c) as obtained from DMEM datasets for the Mg alloy model..... 66

Figure 6. 5 Performance parameter of classifier model (classification report) 67

Figure 7. 3 PCA of healthy rats r64 and r65 (a) PC1 PC2 plot (b) PC2-PC3 plot 68

Figure A. 1 Poster presented used for Conference presentation 74

Figure C. 1 Block diagram for Reflectance measurement..... 78

Figure C. 2 Block Diagram for transmission measurement..... 78

Figure C. 3 Test Sample for measurement in transmission type..... 79

Figure C. 4 AVASOFT GUI interface 79

List of Tables

<i>Table 1: Description of Rats (Wistar) used in in vivo analysis</i>	46
<i>Table 2 Timeline with highlighting different areas covered across semesters</i>	60

1. Introduction

Osteoporosis is a disease that weakens bones, increasing the risk of fractures. Worldwide it is reported to have more than 9 million fractures a year. It means that there is somebody who gets a fracture every three seconds. The highest fracture rates are in Northern European countries. The main impact of such fractures is that they reduce life quality until the patient recover. Additionally, it also increases the financial burden. With changing demography, these expenses are going to rise considerably by 2030.

Bone tissues are unique, as they can heal themselves after damage. Nevertheless, it takes a few weeks to several months to recover based on health and other conditions. Bone healing consumes the patient's time and reduces the quality of life due to strict restrictions on physical movements to aid the healing process. Depending on the nature of the fracture, at times supporting frames like plates and screws are inserted into the bone to avoid deformed healing. If supporting plates/screws are made of biodegradable materials, it would prevent further complications with additional surgical procedures to remove the implants. However, implant interaction with neighboring cells at the interface is complex as it influences numerous factors like the nature of implant materials, its surface topology, and biochemical reaction with living cells. Continuous monitoring of the interface for changes and progressive developments at different time points can assist a doctor in evaluating the progress of implant surgery.

Monitoring implants requires a complex health care system. The optical approach is a low-cost, patient-friendly, and non-invasive technology that shines near-infrared light (NIR) into the region of interest in tissue. The area with and without implant gives the receiver a different spectrum of reflected light due to implant interaction with the surrounding interface. There is an increase in the complexity of biological tissue. Still, variation can help relate the progress of surgery with time at the interface with the help of optical data.

In Europe, extensive research works under the European Union project -MgSafe aims to develop novel imaging technologies using biodegradable magnesium Implants. Ph.D.

candidate, Hafiz Wajahat Hassan, focuses on creating an optical probe to gather information from the magnesium implant tissue interface. He has developed an optical probe that provides NIR spectroscopic data of samples analyzed. The European union researchers in Italy and Sweden conduct studies on animal models to evaluate the interaction of magnesium implants with living tissue (rat-based model) using this probe. Experiments done on animals has their limitations. As part of this thesis, I perform a multivariate analysis from *in vitro* lab experiments to connect to the biochemical changes, such as when an implant is inside an animal body.

1.1 Problem Statement and Research Questions

Integrating biological tissues and identifying experiments to realize the closest resemblance to the magnesium implant tissue interface is complex. The thesis research aims to perform an exploratory analysis to obtain valuable information on the changes near the implant interface as obtained from the optical spectrum data.

The work aims to relate the *in vitro* observations to the *in vivo* datasets based on the problem statement, "**Identify marker that relates¹ changes at magnesium implant- tissue interface, using optical spectral analysis.**"

As part of the thesis following areas, namely the implant interface, optical data-collection, lab experiments for the data collection, and the exploratory model, are studied extensively under the four research questions.

1. Understand properties and features of magnesium implant-tissue interface. What are the possible biomarkers that can directly or indirectly relate to changes near the interface?
2. What are the challenges of optical data collection? Compare commercial probes available at OsloMet to evaluate areas of improvement for the OsloMet probe. Are there new suggestions to improve?
3. Modeling based on human data is beyond the scope of this master thesis. Gather information through (*in vitro*) lab experiments. Relate these trends to a living

¹ Animal model-based lab experiments were excluded initially due to the uncertainty of the pandemic. Fortunately, the animal datasets are available for a more realistic exploratory model, and hence there are modifications to research problem & questions from phase1 report. The four areas of research question are maintained same.

(animal) model. Perform a multivariate exploratory study to relate changes at the magnesium implant-tissue interface. What are the strength and weaknesses of this analysis?

The primary flow of the work is that it introduces *in vitro* experiments performed using DMEM (a cell culture solution). Next is to study the trends and feasibility of gathering optical information, which can be helpful in understanding in-vivo or animal-based experiments. For non-invasive data collection, there is a need for reflection-based measurements. The OsloMet probe, specially designed for animal studies by the MgSafe researcher, is tested with different lab experiments to understand the feasibility of optical measurements. Measurements in an artificial tissue-mimicking gel with two different source-detector distances give optical probe studies considering varying depths. Further, studying dead tissue based on an *in vitro* study gives optical responses to structural changes. This thesis concludes with observations from the optical data analysis on animal models, which have structural information due to implant interactions and functional biological developments due to metabolic activities.

1.2 Structure of Report

The thesis report has different chapters based on the details mentioned above. Chapter 2 includes the literature survey, which introduces the broad area of the research based on existing publications. This section shall introduce the methodology followed for the lab experiments. The following two chapters present differently *in vitro* works with the results and a brief discussion explaining the results' relevance. Chapter 5 details the results from the in-vivo observations. Chapter 6 summarizes the discussions section where the in vitro and in vivo experiments trends. The timeline of works followed by challenges faced and ways to perform prediction models in the future is in chapter 7. The report includes publication and valuable reference information in the appendix. The report ends with a conclusion of the work along with references.

2. Literature review & methodology

2.1 Background

Magnesium deficiency contributes to osteoporosis, weakening bones, and increases the risk of fractures (Castiglioni et al., 2013, p. 1054). Worldwide it is reported to have more than 9 million fractures a year. It means that somebody gets a fracture every three seconds (Borgström et al., 2020). Literature highlights osteoporosis as a matter of concern in European countries within a few decades (Borgström et al., 2020; Castiglioni et al., 2013).

The main impact of such fractures is that the quality of life reduces until they recover. We can calculate a year of one's life using the average health-related quality of life the person had during that one year, referred to as quality-adjusted life years (QALYs). In short, 1 QAL is one year of healthy life. Such a parameter can help measure the disease burden of osteoporosis patients who have a higher tendency for bone fractures. Bone healing may take a few weeks and sometimes several months. Due to osteoporosis, the QALY burden shall increase by about a quarter percentage by 2030, as per a survey done in the five largest European Union countries by International Osteoporosis Foundation (IOF). This rise in QALY lost depends on age, gender, fracture types, patient's health history, days of hospitalization, the level of physical activities, and the healing rate. Additionally, it also increases the financial burden. With changing demography, these expenses shall rise considerably by 2030 (Borgström et al., 2020).

In Europe, extensive research works under the European Union project Marie Skłodowska-Curie ETN MgSafe, aims to develop novel imaging technologies for patients that use biodegradable magnesium Implants. Research on numerous aspects of the implant is progressing in different countries with the help of 15 researchers from various European countries. Ph.D. candidate from OsloMet has developed an optical probe to gather information from the magnesium implant tissue interface. It is possible to collect NIR spectroscopic data from samples analyzed using this probe. Efforts to improve its features and scope of application of the probe are also studied. The European union researchers in

Italy and Sweden conduct studies on animal models to evaluate the interaction of implants inside the rat's body.

Monitoring implants requires a complex health care system. The optical approach shall help develop a patient-friendly, non-invasive technology that shines near-infrared light (NIR) into the region of interest in the tissues. The region with the implant gives the receiver a different spectrum of reflected light due to implant interaction with its surroundings. The interaction depends on the type of implant material used. There is an increase in complexity due to scattering and light specificity in biological tissue. Still, this variation in optical spectra due to the changes and interactions near the implants can help predict the progress of implant surgery. A multivariate model can help to analyze the collected optical data.

Bone tissues are unique, as they can heal themselves after damage. Kim et al. explain how it takes a few weeks to several months (Ding, 2016) to recover based on health conditions and other factors. Bone healing occurs in stages that consume the patient's time and reduce the quality of life due to strict restrictions on physical movements to aid the healing process (Kim et al., 2020). Depending on the nature of the fracture, at times supporting frames like plates and screws are inserted into the bone to avoid deformed healing. If supporting plates/screws are made of biodegradable materials, it would prevent further complications with additional surgical procedures to remove the implants in the same region (Kabir et al., 2021; Kim et al., 2020). When biodegradation happens, the mechanical properties of the materials degrade as the elements absorb into the body through complex biochemical reactions, as illustrated in figure 2.1 (Wang et al., 2020). The changes at the implant interface with the medium of contact can give information regarding the progress of the implant surgery.

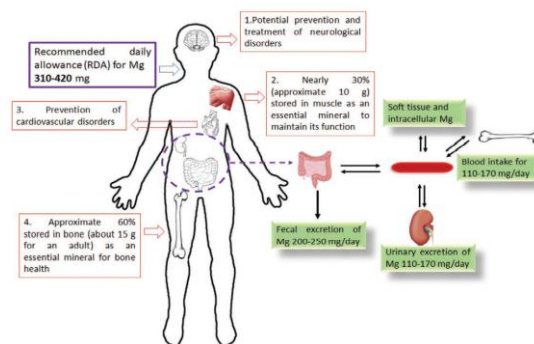


Figure 2. 1 Biocompatibility of biodegradable Mg-based orthopedic implants (Wang et al., 2020) *

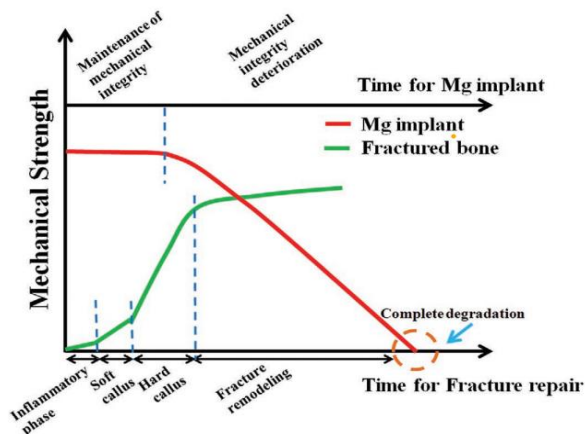


Figure 2. 2 Ideal degradation pattern of the biodegradable fixators to support healing completion at the fracture site. (Wang et al., 2020) *

* are from (Wang et al., 2020) © 2020 The Authors. Published by WILEY-VCH Verlag GmbH & Co. KGaA, Weinheim. (This is an open-access article under the terms of the Creative Commons Attribution License, which permits use, distribution, and reproduction in any medium, provided the original work is properly cited.)

Broadly implants can be classified as non-biodegradable and biodegradable implants. Research done as part of "MgSafe" focuses on magnesium-based implants. It has excellent biocompatibility (Wang et al., 2020) compared to zinc and iron. The mechanical characteristics of magnesium bone screws & pins have properties, namely density and elastic modulus, close to the natural bone. Also, magnesium-based alloys can stimulate new bone formation (Kabir et al., 2021, p. 837). About 60% of total magnesium gets stored in the bones (Castiglioni et al., 2013). There is no surprise that magnesium-based implants found applications in screws, pins, plates, and cardiovascular stents. Thus, magnesium's benefits make it one of the most promising biodegradable substitutes for biomedical applications with more clinical trials (Chakraborty Banerjee et al., 2019).

Unfortunately, pure magnesium has a fast degradation rate that cannot give sufficient mechanical strength until the bones heal. To make them promising for implant applications, usually, magnesium is alloyed. It helps to prevent the fast degradation of magnesium, thereby extending the mechanical life of the implant (Kabir et al., 2021; Liu et al., 2018). Magnesium alloy as implant material has a broad scope of research to improve its properties (Bairagi & Mandal, 2021; Chakraborty Banerjee et al., 2019; Kumar & Katyal, 2021; Radha & Sreekanth, 2017; Tsakiris et al., 2021). Literature suggests that zinc alloying improves

strength, and calcium alloying improves biocompatibility. (Kumar & Katyal, 2021) highlights that these elements have a specific daily allowance permissible for the human body. Also, these elements are present in human bones. As an implant, magnesium-calcium alloy possesses essential biocompatibility and mechanical properties close to cortical bone. As mentioned in the literature, alloying helps reduce the fast degradation rate of pure magnesium implants. It gives sufficient mechanical strength for the bone support until it heals with time (Figure 2.2). To sum up, implant reaction needs to be at slow rates to serve the purpose of its application.

This thesis is an exploratory study based on lab experiments to analyze changes at the implant interface. From *in vitro* experiments, both non-biodegradable and biodegradable are analyzed. Further, animal-based optical datasets make the observations meaningful. The following section explains the methodology for optical data collection followed by the various lab experiments.

2.2 Methodology

The Near Infrared (Near IR or NIR) region falls next to visible light in the electromagnetic spectra. It can pass through the human tissue, making it feasible to collect information regarding changes inside the skin non-invasively. An optical probe is a device that sends light from the source, passes through the medium (specimen), and reaches the detector. The device spectrometer processes this light that reaches the detector as the absorption spectrum. Avantes software AvaSoft with its spectrometer (Avaspec-2048x14, Avantes, The Netherlands) gives spectrum in the range of 650 nm to 1100nm. Calibrate the instrument each time, as detailed in section III of the publication (Hassan, Mathew, et al., 2021). Appendix C1 gives the steps in detail. Microsoft Excel stores the spectrum for further analysis. One of the two ways to capture the optical data from different mediums/days is possible based on the type of medium through which it passes.

2.2.1 Data collection approaches

Transmission type is when the source and detector are on the opposite side of the medium. DMEM solution-based experiment can use this approach without immersing the probe in the liquid. As shown in figure 2.3, place the medium in a cuvette in the optical path between source and detector.



Figure 2. 3 Experimental arrangement for reflection-based measurement done *In vitro* liquid-based medium (a) Path of light in the medium (b) lab set up (c) Illustration of the light source and detector for transmission type of arrangement.

The reflection type is better for a thick medium-like animal surface. It is helpful to collect optical data non-invasively at a certain depth, like from bone implants, without damaging the tissue or medium through which it passes. Light needs to pass through a specific thickness, and a part of it reaches the detector. Based on the required penetration depth, the source and detector are at the required distance on the same side of the medium. Figure 2.4 shows the two different probes used in this thesis. The first probe is a commercially available probe with a distance between source and detector less than 1mm, while the OsloMet probe has one detector and two sources at a distance of 8mm and 6mm from it.

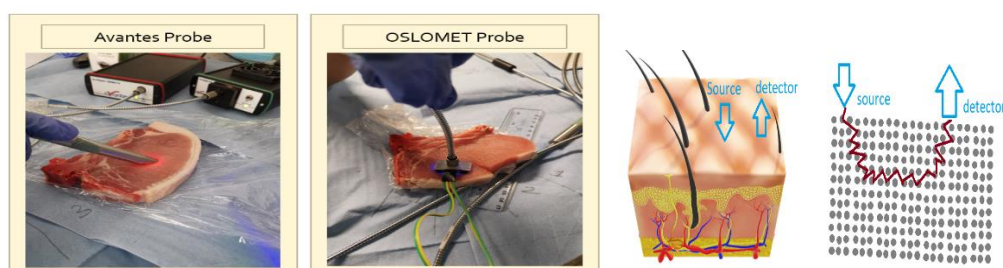


Figure 2. 4 Reflection based measurement (a) Commercial probe (b) OsloMet probe (c) *In vivo* (animal Model) experiments have biological complexity due to the medium

2.2.2 Data analysis

For analysis, prepare the excel by combining all the collected spectrum into a common sheet with additional columns to specify the conditions of each data point. For the exploratory model based on spectrum, the variables are its wavelengths, and the target of interest is the

day when the optical spectra are collected. The optical spectrum from the spectrometer has wavelengths with a resolution of 0.281. Hence obtain the mean value of absorption for a particular wavelength to reduce the number of variables for modeling. On the nature of data gathered, remove both ends of the spectrum to avoid noises from the spectrometer. Preprocess the data based on the pipeline specific to the nature of optical samples. Pipelines for *in vitro* and *in vivo* experiments are different due to the changes in the medium through which light passes. More details are along with the corresponding lab experiments.

Removing outliers or inconsistent data is an important stage of data cleaning. The clustering nature of data samples from a particular sample for *in vitro* and *in vivo* experiments is noticeable in the optical spectrum. However, it was challenging to decide if a particular cluster itself is an outlier. It was with a fear of losing valuable information with limited samples as the thesis focused on an exploratory approach. While modeling, additional care was to consider a particular condition rather than using all available data points. It helps to minimize inconsistent clusters in the model. For example, in the *in vivo* datasets, the first separation was done to consider only magnesium alloy implants from the available data. However, when handled in the same model, the optical information of the right femur and left femur were identified as inconsistent. Thus final animal studies are explicitly done on one femur data sample of rats with magnesium alloy implants. It helps to remove outliers to a large extent. Some points are far away for each day group within this subset. However, as it had information regarding trends, it is retained.

The exploratory model for the thesis uses the popular PCA approach. PCA or principal component analysis is a popular algorithm for dimension reduction. This approach helps to reduce large dimensions of wavelength or number of variables in X, which is close to 400 variables in the experiments done, to n- number of principal components. The highest percentage of information regarding the dataset is present in the first principal component (PC1), followed by the following maximum percent in PC2 until n components. The algorithm generates the principal components corresponding to each data point in the experiment. It is now possible to plot the optical spectra in a new plain of principal components. PC1-PC2 plot and PC2-PC3 plot are two dimensional PCA score plots that help the analysis. With the help of the first three dimensions, it is possible to present as a 3D plot the first three

principal components as well. The explained variance parameter helps to give a quantitative measure of information retainment during the dimensionality reduction. Cumulative variance is a cumulative sum of explained variance that is helpful to express the PCA performance. The loading plot connects the different variables (wavelengths) to various data samples. It unfolds critical wavelengths in the spectrometer range, holding valuable information about the interface changes at each test condition.

The observations and experience from UnscramblerX and Orange3 software helped relate the requirements while working on the spyder available from Anaconda Navigator (anaconda3) to do python programming for data analysis. Python, an open-source software, was used to generate most of the results used in this thesis. Online support for coding and the observations and knowledge from the previous two software platforms were helpful. The python packages and libraries helped reduce the self-coding needed for the data analysis.

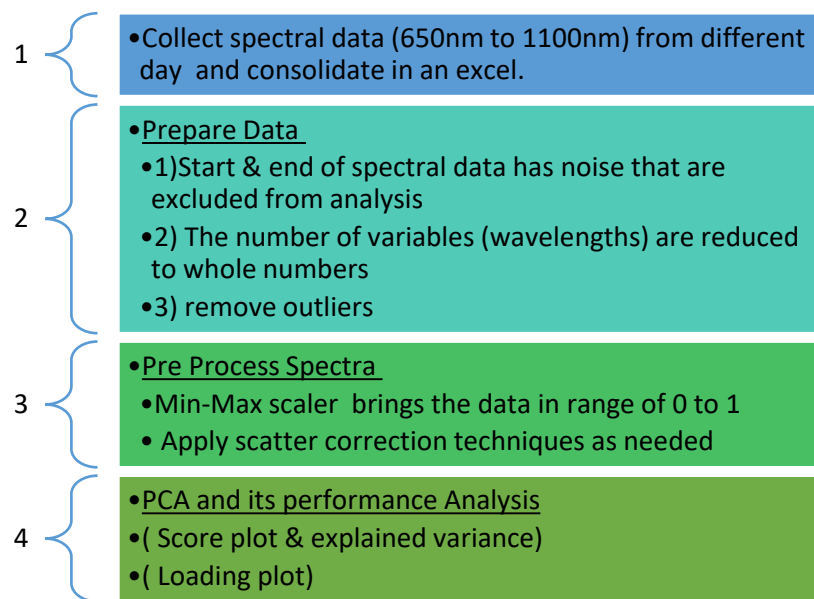


Figure 2. 5 Flow chart for the methodology

Figure 2.5 is the general flow chart for the experiment. The next chapter discusses in detail the different lab experiments. It also discusses the main results from corresponding experiments in the same section.

3. *In vitro* lab experiments and their results.

When light passes through the medium, some light gets absorbed, while some gets scattered based on the medium through which it passes. *In vitro* experiment compares biodegradable and non-biodegradable implant material interface changes as it is in contact with a cell culture medium.

Gibco Dulbecco's Modified Eagle Medium or DMEM is a cell culture medium. DMEM-like liquid medium has low scatters compared to living animal tissues. (Chakraborty Banerjee et al., 2019) compares chemicals blood plasma with cell culture medium including DMEM in table 4 of the paper. Maintaining pH in the medium is with the help of incubator settings in the in-vitro experiments (Luo et al., 2010).

What is pH?

In simple terms, pH expresses if the medium is alkaline or acidic. pH neutral medium maintains its value 7. If the pH is greater than 7, the medium is alkaline, while it is acidic with a pH less than 7. pH range goes from 0 to 14, with the neutral value as seven. By definition, pH is the negative log of hydrogen ion concentration. For an aqueous medium, pH can be in terms of hydroxyl ion (OH⁻) concentration ². The pH meter helps get its value from the DMEM medium during the in vitro experiments.

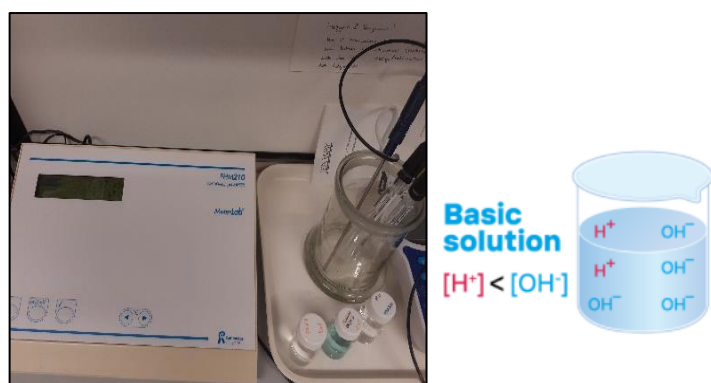


Figure 3. 1 (a) pH meter at UiO (b) pH of a medium is alkaline if OH⁻ ions are more than H⁺ ions

² <http://www.molecularhydrogeninstitute.com/understanding-ph>

Overview of *in vitro* experiments

In the *in vitro* experiment, the pH of the medium on different days is a marker as it changes with time. There are chemical reactions near the inserted material based on the nature of the implant material that is responsible for the changes in pH of the medium. Along with these functional changes, it connects to the interface's structural changes due to the degradation of the implant material with time. This section aims to consolidate the changes near the interface that can help describe the progress of implant interactions for an *in vivo* experiment on live animals.

Preparatory lab work before the actual experiment on the rats by the MgSafe researcher's team in Italy helps learn about the features of the probe. There is a need for an optical probe explicitly designed for this *in vivo* experiment where the rats have an implant placed subcutaneously. Measurements must be 3mm to 4mm range, which is the goal. Experiments 2 and 3 are two different experiments to test the probe's effectiveness using dead tissue and tissue-mimicking gel. Finally, the last section of this chapter discusses the observations from the *in vivo* datasets obtained from lab experiments conducted by MgSafe researchers in Italy, which helps to confirm the studies.

3.1 Experiment setup and data preprocessing

(DMEM based *in vitro* experiment)

Different implant materials interact differently with the surrounding medium. Hence, the *in vitro* experiments learn about implant materials [pure Titanium -Ti, and Magnesium Alloy ZX00 disk [0.45 wt % Zn – 0.45 wt % Ca from BRI.Tech (Austria)] with the help of DMEM medium. As it is a liquid medium, the transmission type of data collection is preferred.

3.1.1 Procedure

Place the disk-type implant material inside a bottle with DMEM solution for this *in vitro* experiment. Prepare three samples for each type of implant. Place the samples in an incubator (TS8056, Termaks) at 37°C with 5% carbon dioxide CO₂ and 21% O₂ (Hassan,

Mathew, et al., 2021). Take measurements on different days from each sample. Day 0 is the reference day before inserting the implant material. Then measurements are taken on the second day, the fifth day, and the tenth day. Take ten measurements from each day for every sample after calibration. For each test case, capturing the light that reaches the detector can give the absorbance value at each wavelength with the help of a spectrometer. The pH meter helps measure the pH of the medium on each condition. An additional test on the implant surface was to measure chemical deposits with a scanning electron microscope (SEM) using the facilities at the UiO laboratory in Norway.

3.1.2 Preprocessing of *In vitro* dataset

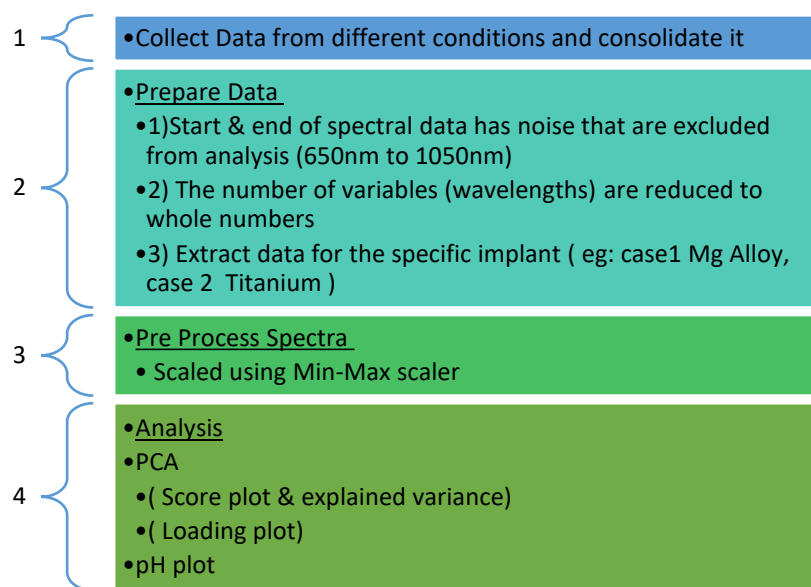


Figure 3. 2 Flow chart for the data processing for the *in vitro* experiment

The spectral datasets provide the absorbance of the samples measured from 600nm to 1100nm. As part of preparing the dataset, remove the last 50nm from both ends to limit the noise introduced from the instrument. The spectrometer provides absorbance data for every wavelength with a resolution of 0.281 nm within the range of the device. These wavelengths are the independent variables or X, based on which we try to study the dependent variable or target variable. Hence we can see that there are multiple variables. Taking the mean of absorbance at a particular wavelength helps to reduce the number of variables to 400. The

measured data had negative readings. As part of data preparation, scale it to a range of zero to one with the help of a min-max scaler.

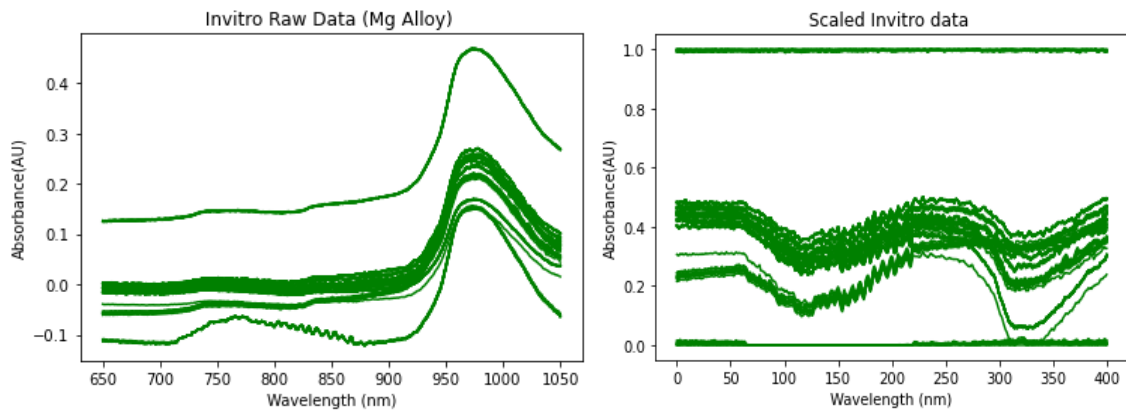


Figure 3.3 Mg Alloy DMEM Data (a) Raw Data (b) scaled data

For more analysis of the datasets, apply the dimension reduction approach after preprocessing. In the work, principal component analysis, also called PCA, is applied to the dataset that helps reduce the multi-dimensions to its corresponding leading principal components. The explained variance is a measure that describes how much information gets retained after the dimension reduction. The cumulative sum of explained variance is a parameter used to describe the total percentage. Moreover, PCA also helps identify the outliers (Figures 3.4 and 3.5). Removal of outliers can help to improve the model further. A comparison of scatter plots based on the score of the principal components reveals some information about the changes in the medium, which redirects to the changes in pH, especially on different days. Hence deciding if it is an outlier is a trade-off. (Sun, 1997).

In the above case study, we see that measurement on day 5 has differences within the samples indicating significant changes in the medium. It is an exciting area to look into from implant interface analysis. However, it raised concerns about proceeding with the prediction model mentioned shortly.

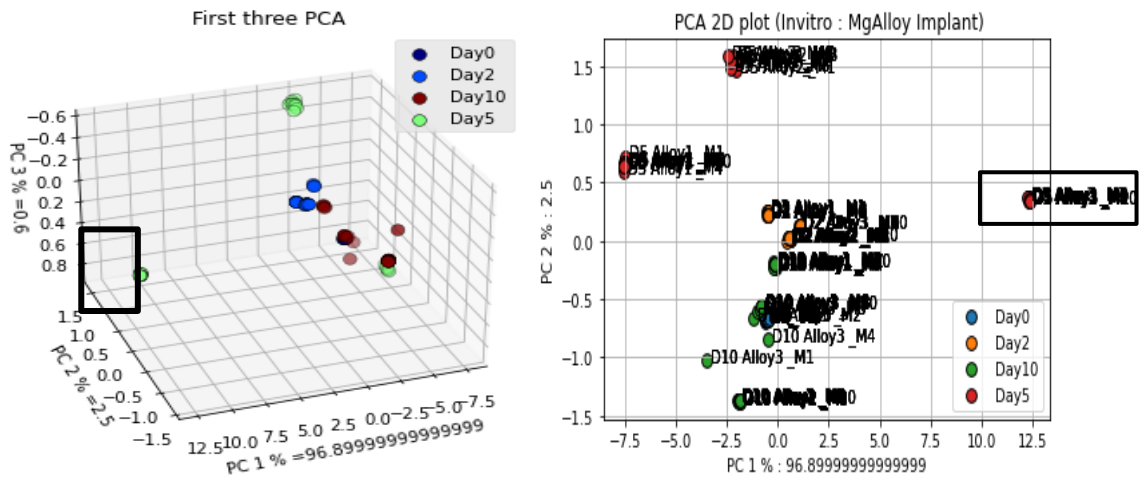
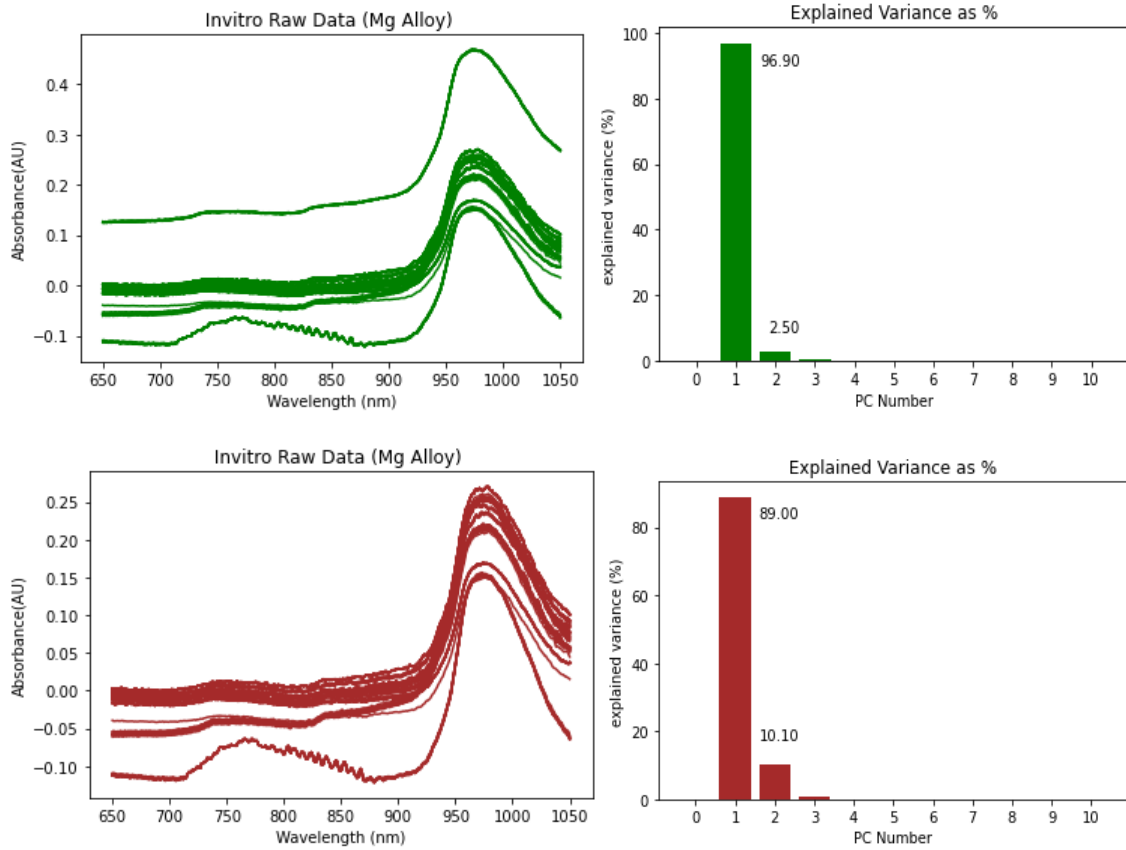


Figure 3. 4 Score plot for Mg Alloy implant material (PC1- PC2) (a) 3 D plot and (b) 2D plot



standard visual assessment tool helpful for measuring wound dimensions. It redirected focus to prediction based on the day as the literature confirms changes at the interface concerning time. There are restrictions on the *in vivo* experiment to collect data every day for the well-being of animals under test. It suggests having sample collection on main days where there is the possibility of the influence. It initiated a piolet study of days 0, 2, 5, and 10 for *in vitro* preliminary experiments and to try classification-based algorithms. It can have performance parameters and a confusion matrix for predicting the multiclass model.

The initial aim was to perform predictions based on the day using the ten measurements on a particular day, with three samples per implant type. Thus, there were 30 data points for each implant material for the DMEM *in vitro* experiment. Likewise, data includes two implant types for the pattern mentioned above on three different days. Hence the *in vitro* DMEM datasets had a total of 190 data points [(10 measurements * 3 samples * 2 implant material * (day2 + day5 + day10) + 10 reference sample].

Initial studies used all the data points. To make the model realistic was my goal. Modeling based on a particular implant type was superior. Such a model is meaningful in the application as a person shall have only one implant for a particular wound. Inconsistent data (or outliers) must be minimal to improve model performance. Thus for use-case-based modeling, the total data points used reduces to one-third. It was a high-impact shrinkage.

The updates on piolet study observations are helpful for future researchers and hence included in the report's challenges section 7.2.3, which covers additional details on modeling and obtaining the parameters.

3.2.1 Trend observed from *in vitro* experiment

Fortunately, this *in vitro* piolet study experiment helped observe an exciting trend in the optical data from the different mediums of the implant. As seen in figure 3.6, it is possible to group the optical spectrum based on data points from each day. Can it be helpful?

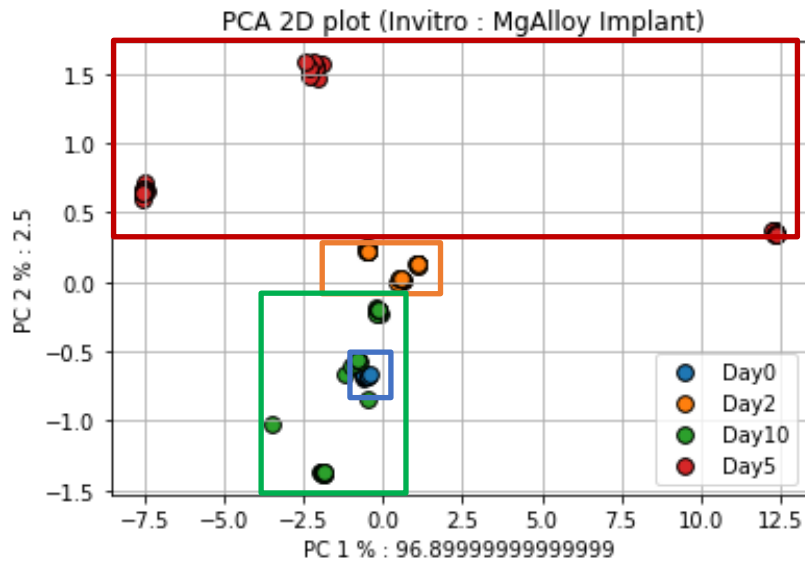


Figure 3. 6 The trend on timepoint based on the complete Mg Alloy implant dataset.

The possibility of separating by the day is exciting as it points to the interaction of biodegradable material with DMEM medium. Day 0 is taken just before the insertion of the implant in the medium. Day 2 represents data points on the second day after the implant interacts with the medium. It is slightly away from the day 0 data points. Day 5 has maximum changes and covers a large area in the PCA plain. The higher positive axis of PC2 separates the day 5 samples. The pH curve (figure 3.7) for *in vitro* experiments for Mg alloy highlights that until day 5, there was a steep rise in the pH of the medium, indicating the reaction changes in the medium due to the presence of the implant material. With time it stabilizes. Day 10 sample points use certain areas in the PCA plain, indicating the continuation of chemical changes in the medium. Of course, the absence of metabolic changes and blood flow of living animals makes DMEM observations different compared with *in vivo* studies. “Efforts to explain different dimensions of this trend are the basis of this thesis.”

3.3 pH curve based *in vitro* experiment

The experiment has different types of implants, namely degradable and non-biodegradable. Magnesium reacts quickly with the medium. As a result, it degrades at a faster rate. This rapid degradation rate of magnesium-based implants is a drawback. It does not help the

bone-implant applications as the mechanical properties of implants should only degrade with time so that fractured bone gets time to heal. A solution to this issue is using magnesium alloy for bone implant applications. After an initial reaction, a protective coating is formed around the surface that prevents fast degradation (Kumar & Katyal, 2021). Hence, magnesium alloys give bone healing time and maintain mechanical support more than pure magnesium implants. Titanium is a non-biodegradable material with minor pH changes among the two implant materials. Unfortunately, as it does not degrade, it requires second surgery when used as an implant material. However, it is helpful to compare with Ti implant in a cell-culture medium to get some reference observations about the range of changes.

Figure 3.7 illustrates the pH graph of each implant material at increasing time points, namely D0, D2, D5, and D10. It shows the pH variation on different days for biodegradable (Mg Alloy) and non-biodegradable (Ti implant material) when placed in the cell culture DMEM medium. Non-biodegradable titanium implant has a rise in pH from day two till day five and later falls to a stable value. On the other hand, the Mg Alloy tends to increase and maintain a higher pH level. The variation pattern of pH is interesting in this experiment as live animal tissues have a slightly acidic pH of near 5 to 6 pH for hairless mice, 6.5 for rats, 5.5 for guinea pigs, 4.1 to 5.8 for healthy human skin rather than an alkaline medium (Proksch, 2018). If so, how does a living animal overcome this shift toward alkalosis?

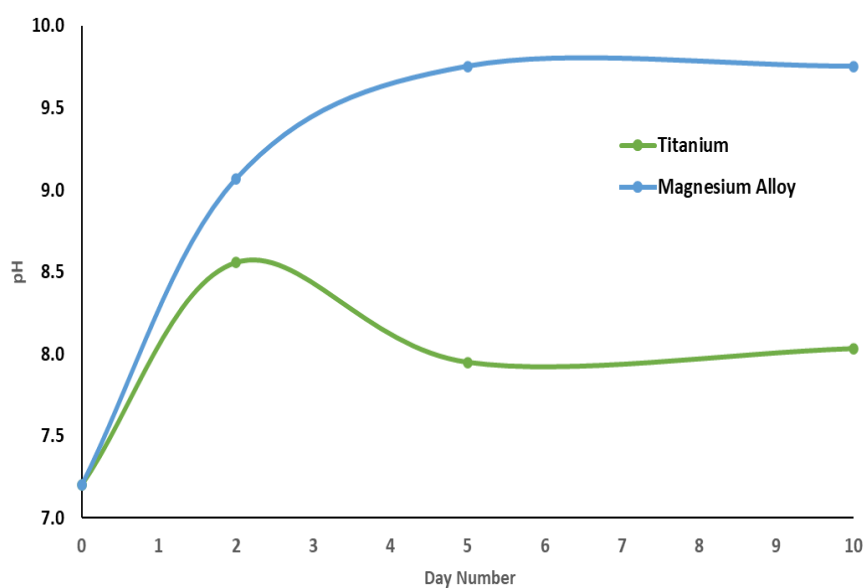


Figure 3. 7 pH of the different mediums on different days. The plot is the average of three samples.

This pH graph is the primary observation for this thesis, as pH can be the biomarker. Unfortunately, getting local pH near the interface for the *in vivo* experiment is not practical presently, as suggested by Willumeit. Studies to draw relation is part of the work.

3.4 A look into non-biodegradable titanium implant

Non-biodegradable titanium (Ti) implant samples can be a reference check. PCA data samples undergo the same preprocessing pipeline as mentioned for Mg implants for plotting. PCA for this group, and the result is in figure 3.8. The goal is to identify similar trends in the titanium dataset.

The higher inclination toward PC1 (explained variance of 93.7%) for Ti implants is due to the day 5 samples. Interestingly, unlike Mg alloy PCA for day 2, Ti implant's sample points are widespread for the second day. It connects to the time points of the Mg alloy and titanium samples changes concerning the pH curve changes. Hence, variations are prominent for Ti implants, especially on days 2 and 5, when the pH rises and reduces to the base value (figure 3.7). This information meant that pH could influence the optical spectrum in the surrounding medium, giving a difference in PCA analysis.

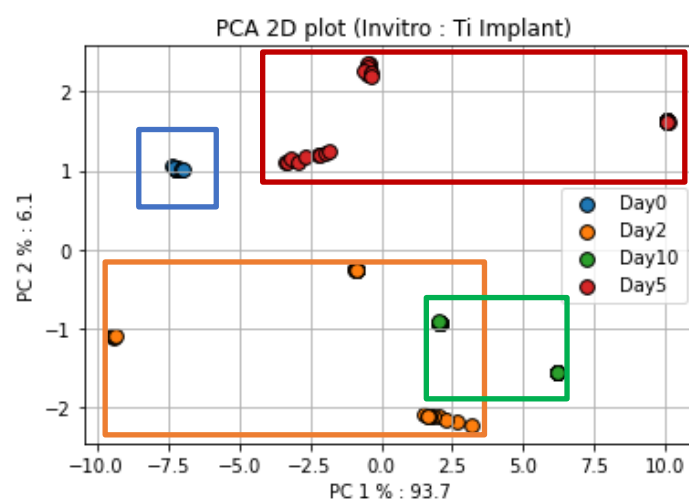


Figure 3. 8 Titanium implant-based PCA

The chemical reactions and changes in the medium are the hidden reason for these optical changes in magnesium alloy and titanium samples. The optical spectrum varies based on the medium through which it passes. Differences in the chemical reaction precipitate formed near the interface in the medium due to DMEM chemical, gaseous chemical byproducts of reactions all contribute to the changes in the light path as it passes through it. Each day has some specific rate of change that distinguishes each day.

To sum up, the trend of separating optical data based on the day is present for the reference non-biodegradable Ti implants and biodegradable magnesium implants, relative to the pH changes.

4. Additional *In vitro* preparatory experiments

(Papazoglou et al., 2006) performs NIRS measurements at 4 different source-detector distance combinations in healthy and unhealthy (diabetic rats) and concludes there is no significant information after a depth of 6mm. For *in vivo* experiments in Italy, there is a need to collect spectral data from the rat's surface with an implant placed subcutaneously after surgery. The probe should measure a depth of 3mm to 4 mm range. The optical probe is designed specifically for the experiment. To get the best results from the *in vivo* test, we (myself and the MgSafe researcher at OsloMet) performed a few lab experiments to test the optical probe before actual experiments. Experiments 2 and 3 are two different experiments to test the probe's effectiveness using dead tissue and tissue-mimicking gel. Before discussing the experiments, there is a need to understand the data collection methodology for *in vivo* experiments. The following section shall explain more about the OsloMet probe and surface-based data collection methodology.

4.1 Probe Studies

The OsloMet probe

As briefed in section 2.2.1, among the two methodologies, *in vivo* measurements need to have the source and detector on the same side of the test specimen, as shown in Figure 4.1. The OsloMet probe sends continuous light from the source. As light passes through the specimen, some light gets absorbed, while some are scattered. The remaining light reaches the detector, which depends on the difference in the medium through which it passes. The light from the detector passes through the spectrometer. The next step is to collect the optical spectral data for data analysis with the help of a computer with AvaSoft software (More details are in section 2.2.2). Calibrate the instrument each time of data collection.

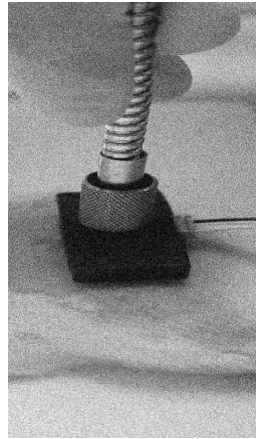


Figure 4. 1 OsloMet probe for reflection-based measurements from the surface.

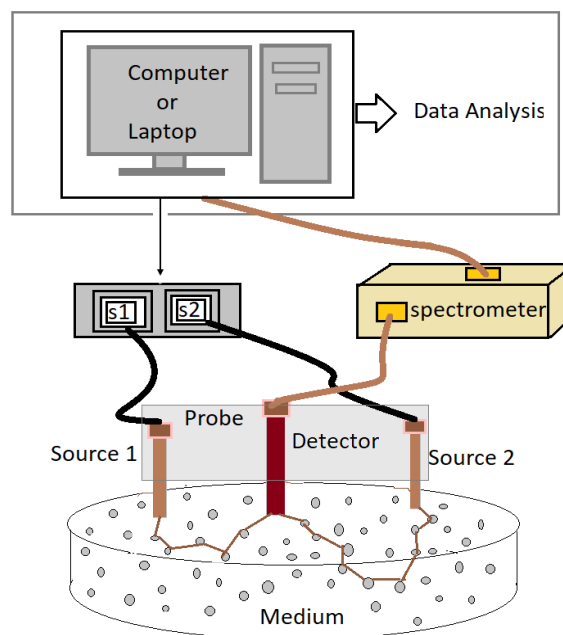


Figure 4. 2 Illustration of optical Probe and Data collection (Hassan, Mathew, et al., 2021)

The optical probe (figure4.1) developed at OsloMet is for specific depth measurement that can help capture spectral information regarding the surgical progression of the implant in animals (rats). The OsloMet probe has two sources and one detector (figure 4.2). The source-detector distance is 8 mm for source s1 and 6 mm for source2. As a thumb rule, the expected data gathered optically is around the depth of $(\frac{1}{3} - \frac{1}{2})$ of the source-detector distance (Papazoglou et al., 2006, p. 1051; Taber et al., 2010, p. 356). The source at 8mm away from the detector is helpful for animal studies.

4.2 Additional *in vitro* experiments

In vivo experiments include restrictions as they undergo defined surgical procedures during the implant surgery, and animal stress must be as permissible within guidelines limits. Hence, there are restrictions on getting invasive measurements. Moreover, additional tests collaborating with other MgSafe researchers from Europe were part of the experiment. Hence daily measurements were impractical on the same rats to avoid stress and unexpected health issues in animals. Thus based on the permissible conditions, data collected by the MgSafe team is used to relate the observations from *in vitro* DMEM experiments. The following prior testing of the OsloMet probe was crucial before the researchers' actual data collection experiment in Italy. These experiments focus mainly on the differences in optical data in different conditions and probe features.

4.2.1 Experiment 2: Dead tissue experiment and its results

Simple experiments on post-mortem pork were conducted in the optics lab to collect optical data from the OsloMet probe and Avantes probe (commercial probe) in the same wavelength range of 600 nm to 1100 nm (figure 4.3). The former gives the surface measurement in a newly purchased pork sample, while the latter gives depth information. (Mathew et al., 2021) .

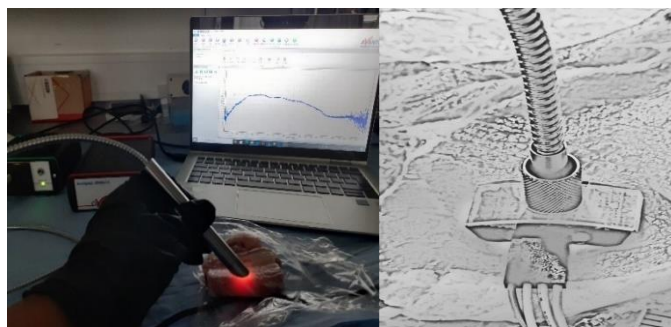


Figure 4. 3 Probe used for experiment (a) commercial Probe manufactured by Avantes (b) OsloMet Probe

This experiment helps to understand the feasibility of separating various tissue of animals. Data was collected using the reflectance measurement approach at 11 selected pork points marked in figure 4.4, including bone, muscle, and different fat thicknesses. OsloMet probe

and commercially available Avantes probes capture reflectance measurement from the exact sample locations.

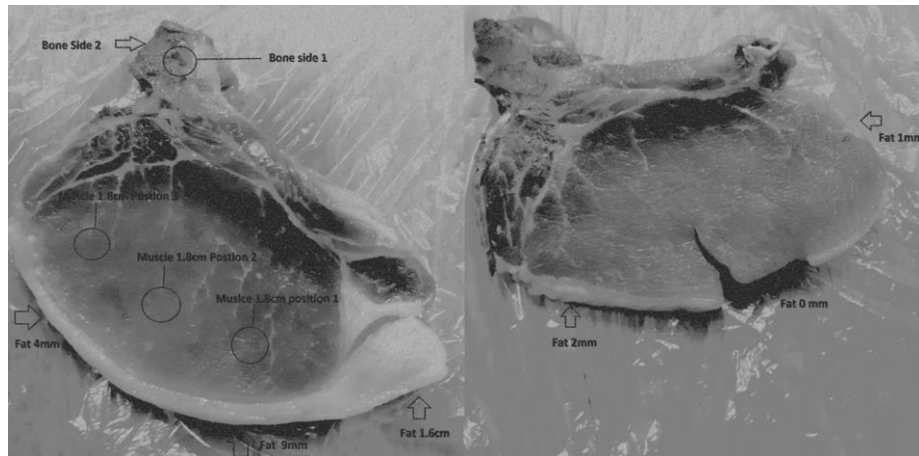


Figure 4. 4 Eleven different selected points

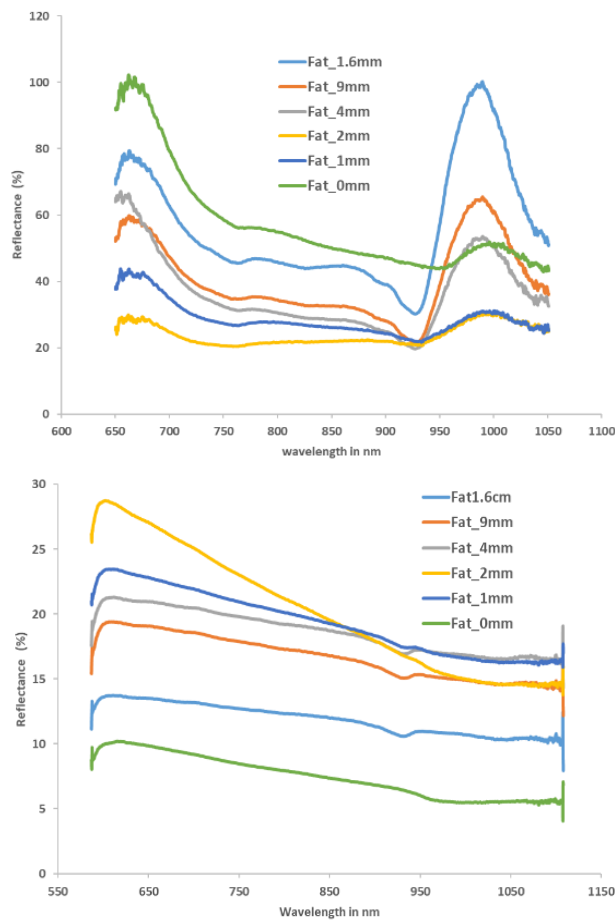


Figure 4. 5 Spectroscopic data plot (a) for varying thickness obtained from OsloMet probe (b) For varying thickness obtained from Avantes probe

OsloMet probe at a source-detector distance of 8 mm compared with data obtained using the Avantes reflectance probe. The OsloMet probe responded to varied height distinctions for varying fat thickness (figure 4.6). This source-detector distance depends on the differential path length factor (DPF), which accounts for the actual distance traveled by photons before reaching the sensor. Scattering properties influence DPF. It confirms that the light reaching detector depends on the medium through which it passes. Interestingly, the probe developed at OsloMet helps distinguish the difference in the medium as light passes through it.

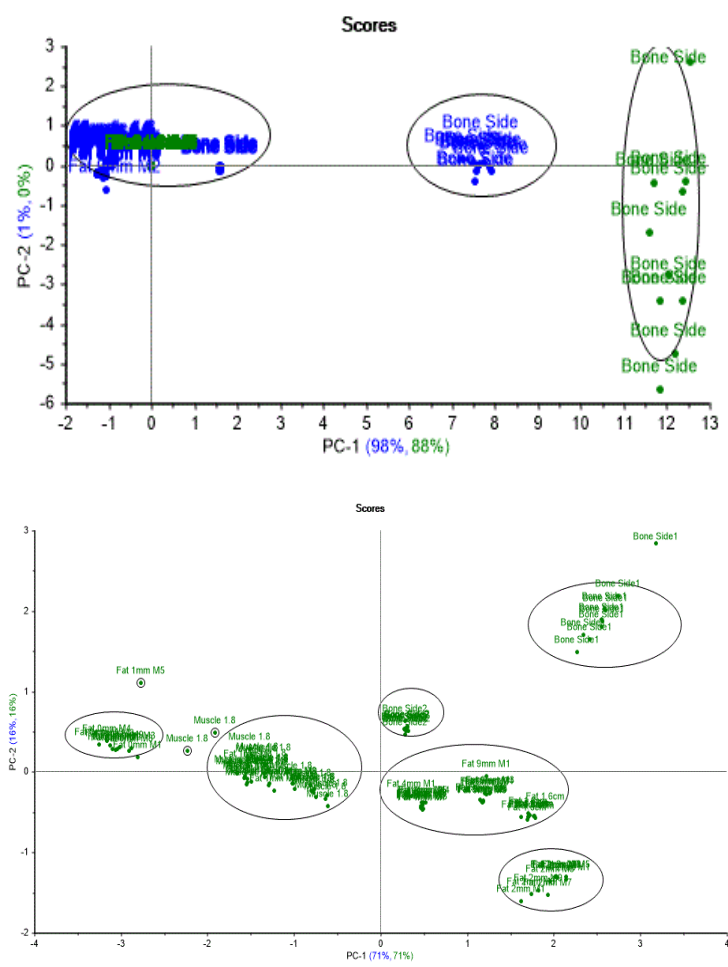


Figure 4. 6 (a) PCA of post-mortem animal tissue Study of Avantes Probe Scatter plot from Unscrambler software (b) PCA study of OsloMet Probe, score plot from Unscrambler software.

The different tissues of pork samples were in the cluster using the Avantes probe as in figure 4.7(a), which uses the significantly less source-detector distance probe to measure. Interestingly, the OsloMet probe can group the different tissues used in the experiment, as

shown in Figure 4.7(b). The probe distinguished the different types of testing mediums that indicated that the OsloMet probe could be helpful for animal studies with different layers of biological tissue beneath the skin.

4.2.2 Experiment 3: Gel Based Experiment and its results

Different implant types were placed in an artificially created tissue-mimicking gel to test optical data received at the detector when illuminated independently from the two sources. (Hassan, Mathew, et al., 2021) explains the process of gel preparations in the chemistry lab at OsloMet. The lab experiment captures information from a particular sample using the s1 source (8mm) and the s2 source (6mm). The goal is to identify the difference in the optical data collected from different implant samples. Additionally, testing from each source helps differentiate measurements from two different depths.

PCA in Orange data analysis software is in figure 4.7. Interestingly, it separated 100% of the data information from source1 and source2. This feature is supportive as the probe can measure data at varying depths in the sample optically. An important observation of this experiment is that it is possible to predict depth in terms of the source to detector distance. (Papazoglou et al., 2006, p. 1051; Taber et al., 2010, p. 356). Alternatively, it gives 100% separation of optical data was 6mm or 8mm depth of each sample set.

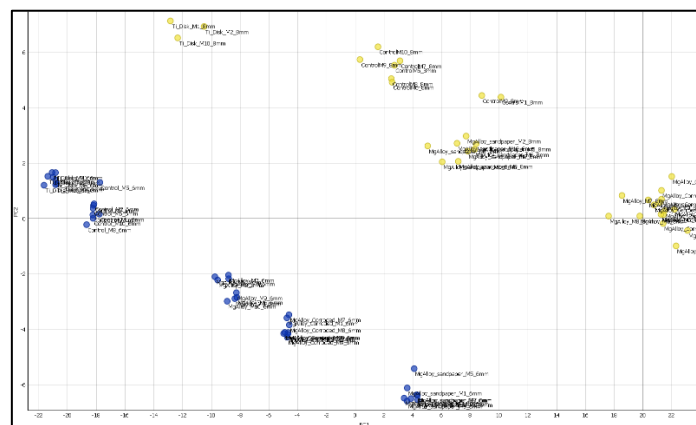


Figure 4. 7 Principal component analysis (PCA) for 6mm and 8mm source distance measurement of optical probe (blue dots are 6mm and yellow dots are 8mm).

Moreover, it is helpful to track the changes at the interface due to chemical reactions with different implant materials. If a particular measurement depth is selected, say 6mm, then

the magnesium alloy-based samples can be separated from titanium and control samples. The difference due to the material's surface when sandpapered/corroded gives a noticeable difference in the plots (Hassan, Mathew, et al., 2021). The possibility is that magnesium-based alloy's chemical reaction gives hydrogen gas near its surface that is absent for implants without magnesium. Hence, the optical measurements include light's effect that passes these gas in the optical path. It is essential to remember that magnesium (or its alloy) degrades to generate hydrogen gas, influencing the optical dataset. (Deni Noviana a, 2016) shows the images of hydrogen gas cavities formed in an experiment conducted on rats with magnesium implantation. On day 7 of implantation, the gas cavities were higher due to the type of implant in that experiment survival study. The gas bubbles formed in the skin were even visible with naked eyes due to the nature of the implant material used for the experiment by Deni Noviana et al. Closed-porous pure magnesium implants were used. (Zhang et al., 2009) uses high purity Mg-Zn-Mn alloy for *in vivo* experiments where the bubble formation was not visible with naked eyes. Hence nature of implant material has a vital role in implant degradation. Hence *in vivo* study uses only one type of magnesium implant material for all rats.

The preliminary lab experiments help prepare for *in vivo* measurements using the OsloMet probe. A commercial probe study highlights the significance of the distance between source and detector as the requirement is to analyze optical changes after light passes through body tissues. Also, tissue-mimicking gel-based experiment highlights that it is possible to separately group optical data at different depths or, in other words, different source-detector distances. Thus, the OsloMet probe can help collect data as needed for *in vivo* experiments. The difference in light absorption from a particular medium is due to changes in the tissues through which it passes. For *in vivo* experiments where the light passes through different layers of live tissues, the optical spectrum shall include the changes in the medium due to variation in the blood (hemoglobin), pH changes near the wound or the interface surrounding, and gas generated due to biochemical reactions. It is interesting to study the *in vivo* datasets, which is the focus of the upcoming next section.

5. *In vivo* experiment results

In vivo experiments focus on biodegradable magnesium alloy implants in rat (WISTAR) models. The NIR light passes through the medium, including fat and hemoglobin, scattering or absorbing it. I was not part of the data collection from animal models. Data is made available from the MgSafe research project associated with OsloMet. The goal is to analyze more physiological and functional changes near the magnesium implant interface. The discussion section examines the trends *in vitro* and *in vivo* experiments more closely. The rat that faced deviations in surgery progress is closely analyzed and compared with the healthy rats to explain the progression trends using the optical data.

5.1 Research Ethics and overview of the dataset



Figure 5. 1 Data collection for *in vivo* experiments

The research experiment was conducted at the Institute of Clinical Physiology, CNR, San Cataldo Research Area, Via Moruzzi, 1, 56124 Pisa, Italy, under the MgSafe project's umbrella. OsloMet researcher was part of the team, and OsloMet owns the rights to control and use the optical data gathered using the OsloMet probe. The data collection was conducted based on the guidelines and protocol for such experiments. The team had a specialized surgeon who led the data collection activities. Special care was to limit the stress on the animal as there was data gathering from other devices apart from the optical probe. Long-term planning and meticulous preparations happened before the actual experiment in October 2021.

Three different implant types are part of the datasets gathered from *in vivo* experiments. To avoid the vastness of the work, I am analyzing rats with magnesium alloy implants as it can

help me gather information near the magnesium implant interface, the ultimate goal of the thesis. A group of four rats has the Magnesium alloy of WE43 implant. A similar implant is inserted in rats' right and left femur bones after a systematic surgical procedure by a surgeon. Measurements at different test points or days help study the progress of degradation over a certain period. Measurements on the same day after the surgery are day 0 data. Measurements are available for day 3, day 7, and day 14 from the primary rat group. This biweekly data is principal analysis. Two rats from a secondary group helped collect optical data from day 45. It is part of the study as a piece of additional information on progress after a few weeks of surgery. However, spectra from the initial time points are unavailable for this group and vice versa for the primary rat group. Relation to the progress of wound healing and changes in metabolism near the wound for rats is crucial as more complex chemical and biological reactions occur due to the interaction of the magnesium implant. Optical information gathered is interesting to investigate and relates to using this as a possible non-invasive medical treatment modality. Preprocess of available data is the first step.

5.2 Preprocessing and the pipeline for *in vivo* dataset

The optical data collected from the animal is the *in vivo* datasets. Due to biological complexity and changes in implant material differences, modeling needs to be on a specific implant target that shall help avoid inconsistent data. Such observations can help create a prediction model for the future. Based on the observation in experiment 3, for consistent data, exploratory data analysis is done on optical spectral data collected from rats with magnesium alloy implants group only through the complete dataset has two additional implant types were also available.

A particular rat has the same implant in the left and right leg. Interestingly, the optical data collected from different body parts are different even when taken from the same rat. PCA-based score plot based on data collected from left and right legs of Mg implant rats is in figure 5.2, which confirms the above comment. The *in vivo* experiments critically observe that their biological changes are different across the body parts, which calls for the model to

be specific to the area of interest. This data analysis is a pilot study; the thesis focuses mainly on one leg, namely the right leg.

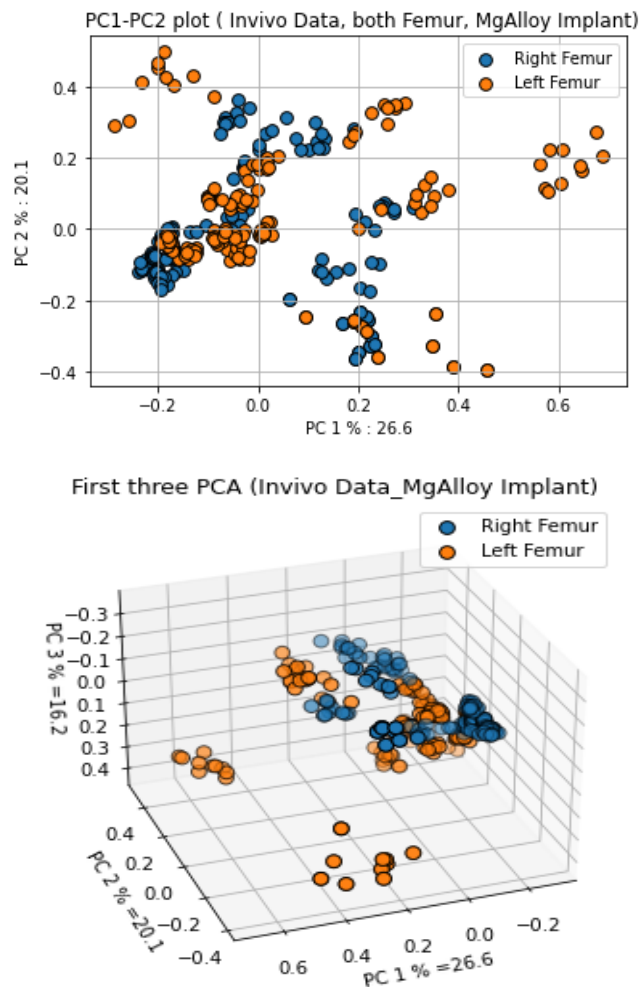


Figure 5. 2 Right and Left femur data points from all-day conditions for Mg Implant Rats (a) First two PCA (b) First 3 PCA. Left femur data have more outliers compared to right femur.

The first step of processing animal data is to separate the required conditions like magnesium implant data from the right femur of the rats. Same as in the *in vitro* data, reduce the number of observations by taking the mean of amplitudes per wavelength. Avoid the extreme ends of the spectrometer range to avoid noisy data points. Compared to *in-vitro* data, the *in vivo* data has more negative readings. To retain the information, perform min-max scaling. Unlike the *in vitro* datasets, PCA did after the above stage was not giving any detailed information regarding the trends.

The *in vivo* optical data collected from live animals with different layers include fat, skin, muscles, and blood flow. The fat tends to scatter light while hemoglobin in blood absorbs

NIR light. (Rosen et al., 2002). Additionally, due to the interaction of magnesium implant, there is a reaction that causes biological changes in the vicinity, including changes in pH, also referred to as wound pH due to surgery. The hydrogen gas formed as part of the implant reaction occupies the regions near the implant (Deni Noviana a, 2016). The gas bubbles near the implant can slowly increase in dimensions as they come closer to each other. Such bubbles influence the optical information due to light scattering as it falls in the light path. As the primary goal is to understand the changes at the interface, this bubble formation helps gather internal changes near the implant. Also, body healing after the surgical procedure adds more changes at the cellular level as many dead cells start to form in the upcoming days of the post-surgery period. Hence the optical information gathered from the surface above the implant is the net effect of complex biological changes. It needs further processing to identify the information regarding the implant surfaces. As the wound heals, there are changes in the skin wound. Local tissue changes influence optical properties (Jayachandran et al., 2016).

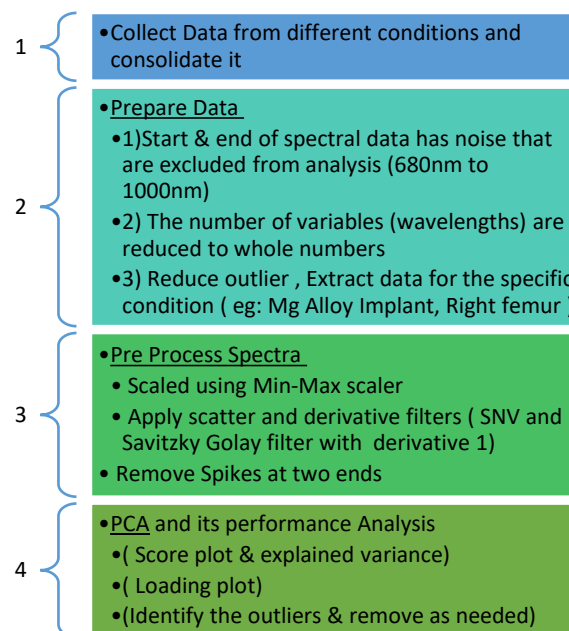


Figure 5. 3 Flow chart for the data analysis for the in vivo experiment

After repeated close analysis of filters and their application order, I observed trends similar to *in vitro* data in the PC1-PC2 plain that separates the optical data to different time points. Figure 5.3 shows the preprocessing of the *in vivo* data flow, which helped me see the trend.

Unlike the DMEM *in vitro* data analysis pipeline, it uses two other preprocess approaches: a scatter technique known as standard normal variate or SNV and a derivative filter.

Multiplicative scatters correction (MSC) is a popular scatter technique (Prieto et al., 2017). But it needs a reference spectrum that is ideally free from scattering effects. Getting such a spectrum is not possible in this case. A popular approach uses the mean of the sample data spectrum, but it reduces performance under the influence of outliers. Due to complex changes in the medium, there are possibilities of inconsistent data at someday points. Due to minimum sample points, removing data as outliers is not a good choice to study the trend as they have helpful information even if it spreads in the PCA plain (Sun, 1997). It motivates me to try another scatter technique, SNV or Standard Normal Variate, which performs on each spectrum. In this technique, it divides the mean-centered spectrum by its standard deviation³ $Xi_{snv} = \frac{Xi - Xi_{mean}}{\sigma}$. Interestingly, it groups the spectral data collected from different days. Compared to *in vitro* datasets, the overall optical datasets highlight the variations. A derivative approach can help to capture the changes in the spectrum. Hence the derivative technique Savitzky-Golay filter (Sun, 1997) with derivative 1 is applied to the dataset. In the last stage, remove the spikes at the ends to avoid high explained variance on PC1 during the subsequent analysis stage. The *in vivo* input and final preprocessed data are in figures 5.4 and 5.5. Hence additional preprocessing is needed for invivo data (Fan et al., 2018), after which it passes to the next stage. PCA is on this preprocessed data, as detailed in the next section.

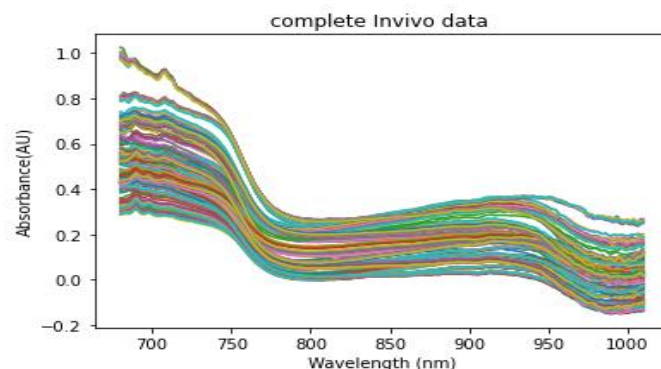


Figure 5. 4 Raw *in vivo* data as obtained from the spectrometer for Mg alloy Right implant

³ <https://towardsdatascience.com/scatter-correction-and-outlier-detection-in-nir-spectroscopy-7ec924af668>

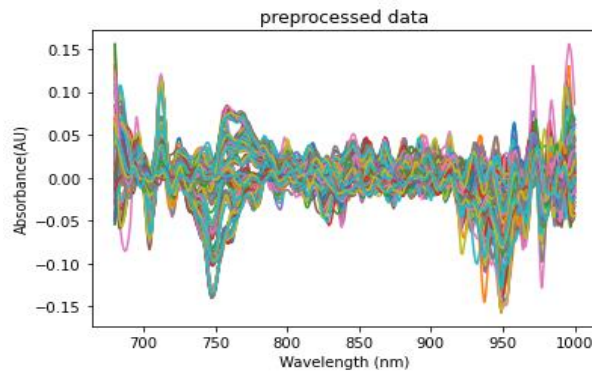


Figure 5. 5 Preprocessed data by the end of step3 in the flowchart. It is the input for PCA analysis

5.2 Principal component analysis (PCA) of *In vivo* Data

With the information on the test conditions, let me continue the PCA analysis of *in vivo* datasets. After the preprocessing, the required variables pass through the PCA dimension reduction process. For *in vivo* samples, the total number of variables is from 680nm to 1000nm, of about 320 variables. It is not practical to plot 320 variables (multivariate data) into a plain so that a human being can visualize it. These 320 variables are reduced to 10 principal components, retaining a certain percentage of information referred to as the explained variance. Individual and cumulative percentages of explained variance are in figure 5.6 for the first 10 components.

PC	Explained Variance	Cumulative Variance
0	0.0	0.0
1	PC1	39.5
2	PC2	26.4
3	PC3	11.4
4	PC4	3.9
5	PC5	3.2
6	PC6	2.4
7	PC7	1.5
8	PC8	1.3
9	PC9	1.0
10	PC10	0.9

Figure 5. 6 Explained Variance of PCA in figure 5.7

After reducing the dimension, the first principal component has 39.5% information, and the second has 26.4%, making a total of 65.9% while plotting the scatter plot as in figure 5.7. Adding the third principal component retains 77.3% of information (figure 5.8). The first three components carry most of the information in this *in vivo* dataset.

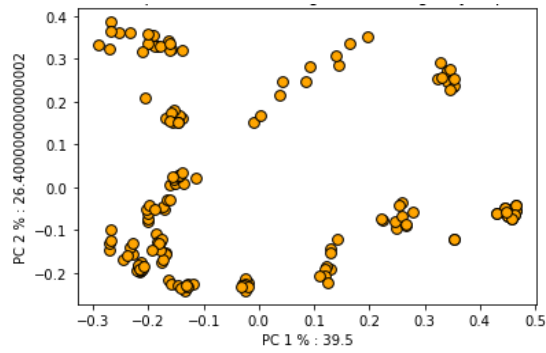


Figure 5. 7 PCA of MgAlloy implant-based optical data-based PCA of the right femur. The first two PCA plotted in the 2D plot

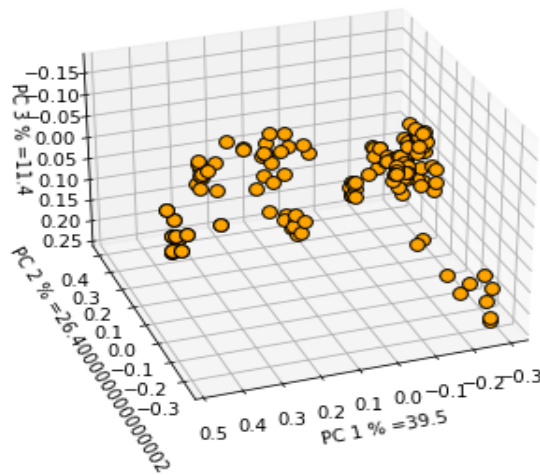
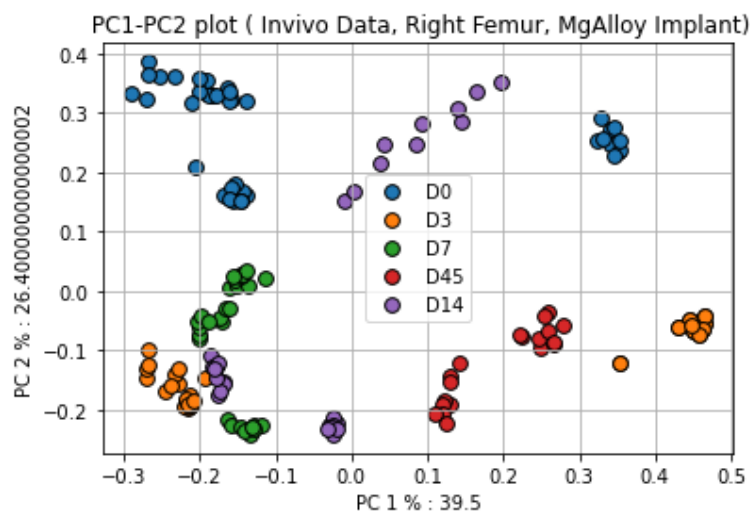


Figure 5. 8 PCA of MgAlloy implant-based optical data-based PCA of the right femur. The First 3 PCA components plotted in the 3D plot

Thus, preprocessed Mg Implant optical spectrum from Right femur datasets retains 77.3 % of the information when considering PC1, PC2, and PC3. Unlike the in-vitro data, the explained variance is exceptionally high compared to PC2.

- Does the PCA of optical data from the rats on a different day tell us any information?



•

- Figure 5. 9 PCA concerning PC1 and PC2 based on different days

The next stage is to perform a detailed analysis of the different conditions and look for the trend from *in vitro* data. This section includes efforts to understand the difference in optical data for different rats. Let us observe the same plot in figure 5.7 from the angle of different days (figure 5.9). Day 0 (D0) has a significant cluster and a small cluster separated from this leading group. Similarly, day 14 (D14) has two clusters close by, while one stands out from these.

Interestingly, timepoint 3 has two separate clusters. Why is the gap between the two clusters so much? Both clusters represent the optical information of rats at the same time points, which means the changes in the medium through which the light passes are similar, giving the same expected reactions inside the rat's body. Of course, slight variation based on the difference in rats is normal. But why are the two significantly separated clusters formed?

5.3 Additional details about the rats used in the Model studies

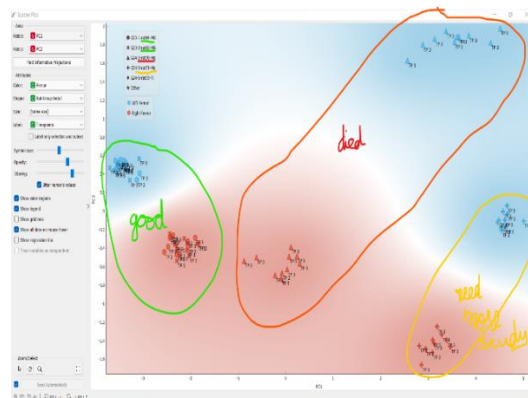


Figure 5. 10 Initial Orange-based observations

Preliminary observations in Orange 3 software separate the left femur from the right for time 3 is interesting as it also gives similar results but in a magnified approach (the difference is due to changes in normalization of widgets in orange software). It gives additional information on the different rats used for the analysis. In the red region (right femur datasets) of the orange software-based results of figure 5.10, the rats 64 and 65 are grouped into a cluster, while rats 70 and 71 are separated further away from the initial groups. A similar trend is in the left femur, but points are further apart.

Before proceeding with the PCA results, it is essential to familiarise the samples or rats used for the discussions. From the information gathered from the researcher, one rat (r70) died on day 3 and couldn't survive the surgical procedure. Hence we have data until day 3 for this rat. For the remaining rats, data is available for day 0, day 3, day 7, and day 14. Day 0 gives optical spectra of changes soon after the implant interaction with the living tissue. Days up to a fortnight are of primary interest as it helps to relate to the *in vitro* experiment. Day 45 is a piece of additional information in PCA analysis.

A particular rat could survive the surgery, but the spectral data was not the same as that for unknown reasons. Hence this rat is also of interest. The thesis is now challenging within *in vivo* datasets and finds areas to explore as the research progresses. For a quick sum up, summary information regarding all the rats is in table 1.

Table 1: Description of Rats (Wistar) used in *in vivo* analysis

Sl.No	Reference used in the report	Rat group with Rat number	Weight	Data points	Preliminary observation
1	r64	(G23 -1 –rat 64)	218 g	Day 0,3,7,14	Survived the implant surgery & Normal
2	r65	(G23-2 –rat 65)	224 g	Day 0,3,7,14	Survived the implant surgery & Normal
3	r71	(G24-3-rat71)	225g	Day 0,3,7,14	Rat survived the implant surgery. Did it have differences observed from the Orange 3 data analysis? It needs a detailed analysis in the discussion section.
4	r54	(G21_1_rat54)	249g	Day 45	Day 45 data only
5	r57	(G21_4_rat57)	243g	Day 45	Day 45 data only
6	Rat 70	(G23_rat70)	230 g	Day 0 , 3	Died on day 3

The PCA analysis in figure 5.11 highlights the rats that have survived after the surgery. It can answer the questions discussed before. The samples collected from rats 64 and 65 were healthy clusters with day points in the color code. At the same time, the rat 70 (dead rat) and rat 71 (unhealthy rat) are the far-away clusters.

- Can the optical data of the dead rat explain any hidden message?
- Can optical data guide in understanding the health on different days?

From day 0, the rat with unhealthy conditions is separated in its PCA plain. Day 3 is very much exciting and critical. The two healthy rats are on two opposite sides of PC1 in the PC1-PC2 plain. The optical spectra collected from these rats (r70 and r71) differed from healthy rats (r64 and r65), as in figure 5.11. As the next step of this exploratory analysis, let us analyze the wavelengths that contribute to optical information.

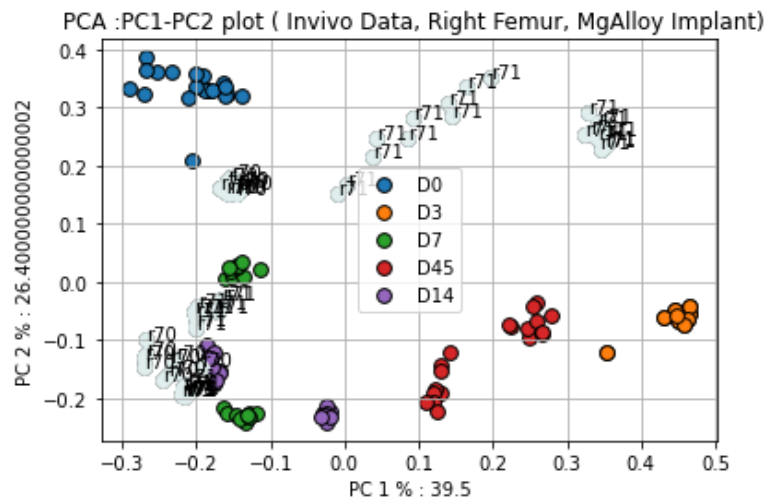


Figure 5. 11 PC1 -PC2 plot highlighting different timepoints where the unhealthy rats are in white with label

5.4 Wavelengths of significance

A loading plot in the PCA is helpful. It relates additional details in the datasets. Loading-plot in the PCA can relate to the features in the datasets (Westad et al., 2003). In the spectral datasets, features are the wavelengths. The figures in 5.12 and 5.13 help in primary feature selection. The plot highlights that wavelengths near 680nm, 720nm, 750 nm, and 775 nm are of interest at the beginning of the NIR range, which strongly influences absorption due to hemoglobin and cytochrome c oxidase. Oxyhemoglobin absorption rises while deoxyhemoglobin reduces in this region, and metabolism-related changes (cytochrome C oxidase) have had their peak prominence at around 800nm (Taber et al., 2010). The higher absorption after 940nm is another area of interest concerning light absorption by water in the medium. Below the 1000nm range of NIR spectroscopy, wavelengths 955nm and 995nm seem to carry some information. The region above 1000nm gives more water content in the medium or tissues.

As mentioned in preprocessing section 5.2, the derivative 1 filter is used that helps to highlight the wavelengths that are having changes in the raw spectra, as discussed

elaborately in (Sakata et al., 2012). The author, with images, explains how the slow rise in absorption curves and the sharp changing peaks in derivative curves of spectra. The amplitude of the sharp peaks is proportional to the changes in the actual spectra. Figures 5.14 to 5.17 use the preprocessed *in vivo* data from one of the measurements to plot the graphs for different days. It is the derivative spectra of *in vivo* data. Though the availability of data samples is a limitation, it can be helpful to see an opportunity for a comparative study. It helps to identify the wavelength that influences more closely.

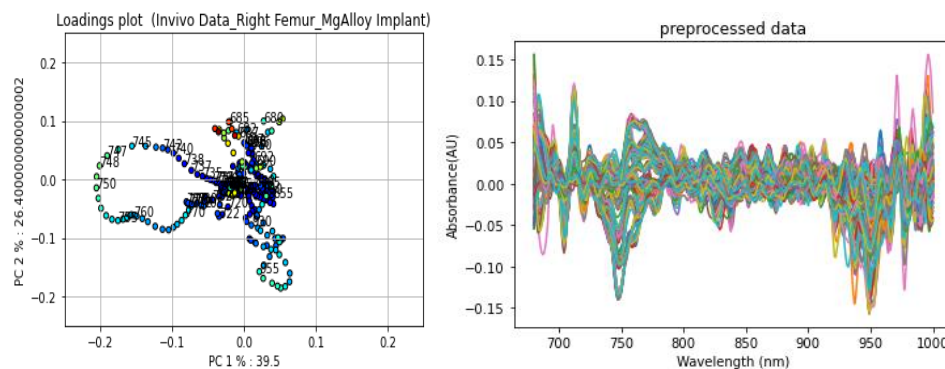


Figure 5.12 Loading plot and preprocessed optical data from the right femur of all rats having Mg implant

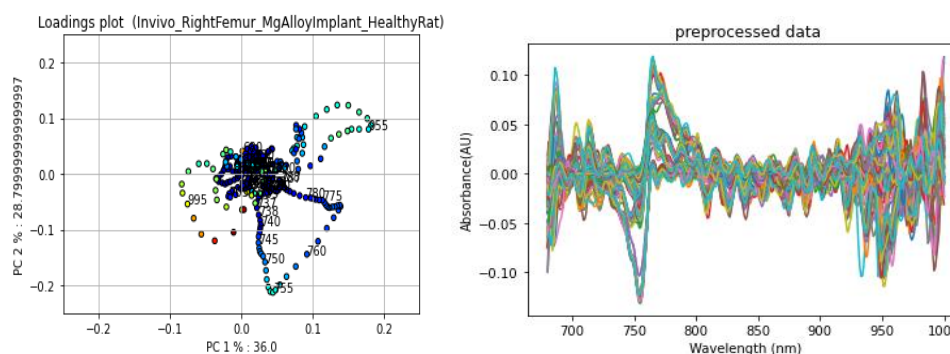


Figure 5.13 Loading plot and preprocessed optical data from the right femur of healthy rats alone

Day 0 refers to the optical samples collected on the same day after surgery. Hence the magnesium implant starts to interact, giving optical changes. Additionally, the animal responds to the metabolic changes near the wound after surgery. Hence rats have maximum differences in the optical data, as in figure 5.14. All rats have similar hydration changes with peaks at 950nm, while changes due to blood flow in the region near the interface are different for each rat as in regions from 680nm to 800nm. Interestingly rat 71 has maximum differences.



Figure 5. 14 Derivative spectra of day 0

As in figure 5.9, the PCA analysis data point on day 3 are separated 100% in the PCA for healthy and unhealthy rats. Derivative spectra for the same day in figure 5.15 explain that both the healthy rats exhibited a particular optical spectrum that was similar and overlapped. Hence it can be considered a reference to compare the other two rats on day 3. Rat 70 was dead on day 3. The remarkable change from healthy rats to unhealthy rats on day 3 is worth noting in the plot. Derivative spectra of optical data near unhealthy rats' wounds indicate that the hemoglobin and cell metabolism [figure 3 (Taber et al., 2010)] vary tremendously in the opposite pattern from healthy rats, especially from 700nm to 900nm. Also, rat70 has some differences in the 965-975nm range, where water absorption is predominant. It is evident that rat 71 also has significant hemoglobin and cell metabolism issues near the wounds. NIR light's deviation in hemoglobin absorption is striking for the dead and unhealthy rat. It is an indicator of the negative progression of surgery. Though the non-availability of a vast number of animal samples is a limitation, this pilot study can be helpful to see an opportunity for future researchers. This paper focuses on opening the possibility of a promising future for optical diagnosis. A non-invasive technology that doesn't destroy the tissue but at the same time gives varied optical spectra for unhealthy conditions.

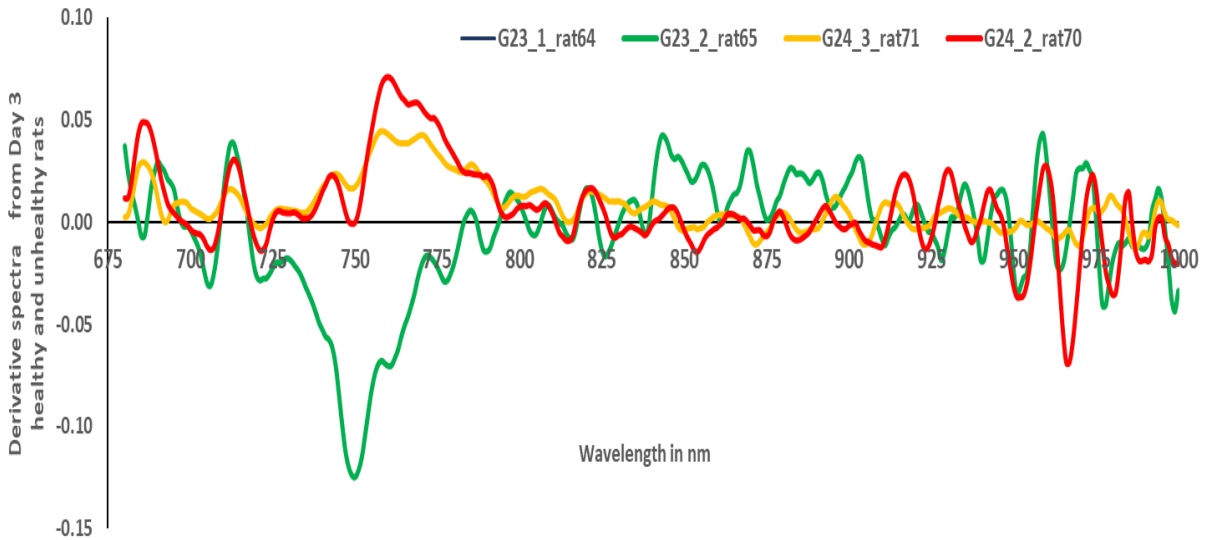


Figure 5. 15 Derivative spectra of day 3

After day 3, there are only 3 plots as rat 70 was dead. Day 7 plots are almost similar, with some differences in magnitudes. As in figure 5.16, some curiosity arises regarding rat 64 primarily related to hydration near the wound and blood flow near the implant interface. (Deni Noviana a, 2016), mentions that maximum internal changes due to wound and implant reactions happen on day 5 (figure 6.3A). So after day 7, the reactions expect to be stable. On day 14, the healthy rats are almost the same, while rat 71 has a higher amplitude in their derivative spectra (figure 5.17).



Figure 5. 16 Derivative spectra of day 7

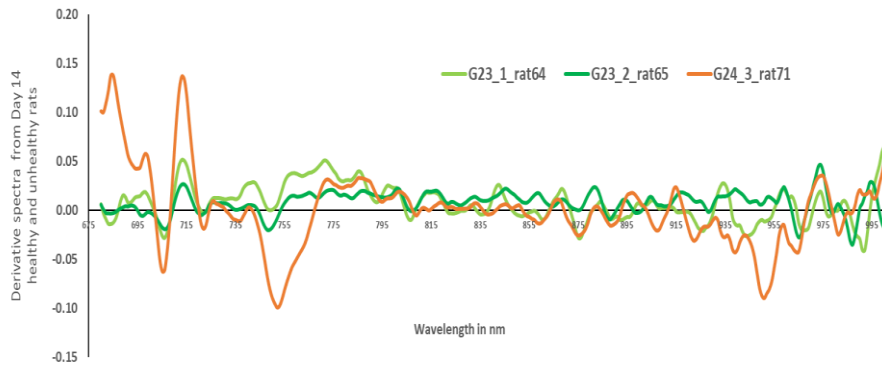


Figure 5.17 Derivative spectra of day 14

Interestingly, the optical probe can distinguish the wound healing near tissues as the peak of the derivative spectra. Keeping in mind the work limitation, I wish to note some exciting wavelengths in the spectra that give information on surgery progress. In this in vivo study, wavelengths of interest are (685, 700, 705**, 715*, 750***, 773, 785), (800, 840*, 855, 870, 885, 905), and (940, 950**, 960, 965-975 ***, 975*, 985*, 995), with * indicating maximum importance in each group.

All these animals survived the two weeks of observation, so rat 71 has some health issues even though it survived. Further examination of images taken during the experiment showed that rat 71 had rashes near the wound, unlike the two healthy ones. The difference in tissue near the wound is the reason for the difference in optical spectra for the rat 71. The following section discusses the possible reasons for issues near the interface.

- What is the reason for the positive trend in surgery progress separated with the help of optical data near the magnesium implant interface? What can be the biochemical changes near the interface?
- What is the future scope of this pilot study?

In the next section, let us revisit the problem statement with detailed discussions concerning *in vivo* data samples compared to *in vitro* results.

6. Discussions

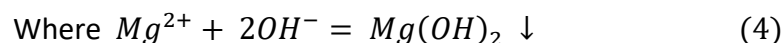
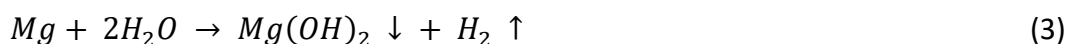
In vivo experiments refer to data from the living body; unfortunately, there is no non-invasive approach to measure local pH to give actual figures to mark the changes near implants (Willumeit-Römer, 2019, p. 1448). *In vitro* data analysis using DMEM medium-based experiments is limited because they cannot directly relate to the pH *in vivo*. However, the trend in pH is interesting to analyze further. pH plotted against different days is fascinating. It highlights the strong relation of implant material with pH on different days. Hence, local pH is a biomarker closely associated with the progress of implants *in vivo*. Let us try to see some chemical equations to relate the reason for changes in pH near an implant surrounding.

6.1 The biomarker pH

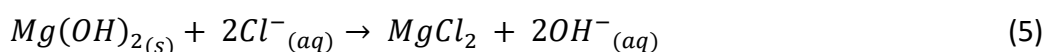
When magnesium reacts with water in the tissue, it produces hydrogen. The equations below explain the changes in the interface (Bairagi & Mandal, 2021; Willumeit-Römer, 2019).



Then the overall reaction can be written as equation three from equations 1 and 2.

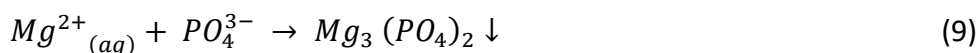
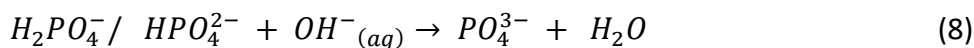
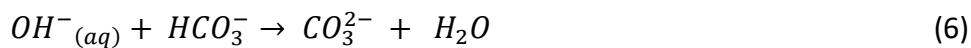


These $Mg(OH)_2$ Alternatively, the hydroxide layers cover the magnesium surface. However, due to its instability, it reacts with the chloride ions of human body fluids for *in vivo* experiments and DMEM medium for the *in vitro* experiment to form highly soluble magnesium chloride, as represented in equation 5.



6.1.1 What is pH?

The pH of a medium is the concentration of hydrogen ions (H^+). The exact pH can also be as OH^- Ion concentration value here. A solution is said to be alkaline or basic if there is an increase in the concentration of hydroxide ions (OH^-) that is numerically the same as a decrease of (H^+). The reaction presented in equation 2 suggests that local pH near the interface shall increase due to the expulsion of hydroxide ions (OH^-). The biochemical reactions are highly complex. As the reactions proceed at the interface, these hydroxide ions help form some precipitates, as mentioned in equations 6 to 11. Thus there is a delicate pH balance near the implant surrounding.



Calcium also reacts to form its precipitates



As from equation 3, water is used to initiate the reaction. On the other hand, in equations 6 and 8, water is a byproduct of the reaction. Thus, as the complex biochemical reaction occurs near the implant interface, there are changes in the presence of water. The volume of water for *in vitro* experiments and the local hydration of the animal body can be biological changes near the interface.

Additionally, corrosion or degradation of magnesium gets fastened due to the disappearance of the hydroxide cover of magnesium $Mg(OH)_2$. As in the overall reaction equation, 3, hydrogen gas is present adjacent to the implant. The literature explains that hydrogen gas's presence is only in the first post-surgery week. In 2-3 weeks of the *in vivo*

implant surgery, the gas gradually disappears and assumes it does not interfere with the healing process if the corrosion rates are within certain limits, especially in the first couple of weeks (Chakraborty Banerjee et al., 2019). Hydrogen molecules are neutral and hence do not contribute to local pH. Equations 7,9,10,11 suggest the formation of precipitates near the interface that can form a coating near the implant that helps reduce the degradation of the implant (Bairagi & Mandal, 2021; Tsakiris et al., 2021). This layer obstructs the interaction of implant Mg with water and helps control the formation of hydroxide ions that contributes to pH. Variation in pH in the medium near the vicinity of the implant is an area of interest.

The body maintains a pH close to 7, neutral. pH greater than seven makes medium alkaline referred to as alkalosis, in which the tissues cannot exist. Hence, pH due to alkalosis can damage cells in its areas of influence. This section concludes that pH is the biomarker of interest as it can decide implant surgery's progress when related to actual implant surgery for living tissues.

6.2 Chemicals at the interface

In the *in vitro* experiments conducted at UiO, additional experiments help study the implant surface. Surface scanning the implant each day using the SEM machine gives a quantitative measure of chemicals present in the *in vitro* DMEM-based experiment. Figure 6.1 highlights the changes of different chemicals on various days. There is a strong prominence of magnesium across different days. Interestingly, it is maximum on day 0 and reduced with time to reach the lowest on day 5. It indicates faster degradation of magnesium in the initial days till about the fifth day. During these days, oxygen slowly but steadily rises. After day 5, the oxygen present is almost stable, and magnesium reaction rates start to pick up slowly but slowly.

As in equations 7, 9,10, and 11, some precipitates are formed in the chemical reactions. These include the $MgCO_3$, $Mg_3 (PO_4)_2$, $CaCO_3$, $Ca_3 (PO_4)_2$. Calcium, phosphorus, and carbon presence in the scan are due to the precipitates settling near the implant surface. Among these, calcium and phosphorous are present across the days. While it is interesting to note that carbon presence increase between day 2 to day 5. Drop after day 5 can be due

to the reduction in carbonate-based precipitates, while phosphate-based precipitates continue over extended periods. (Zhang et al., 2009) mentions the formation of phosphorous precipitates after a few weeks of implantation of magnesium implant in an *in vivo* analysis.

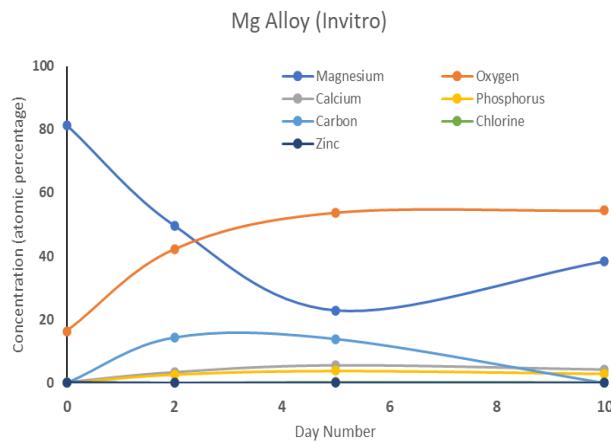


Figure 6. 1 Variation in the presence of different chemicals near the interface

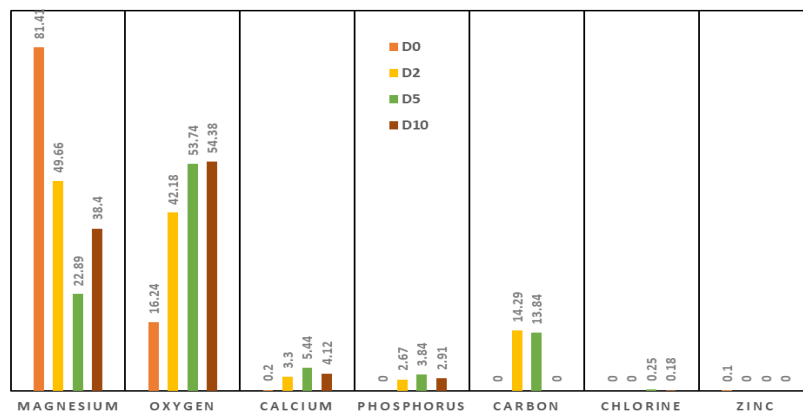


Figure 6. 2 Summary of Elements present in the Magnesium implant surface from in vitro experiments.

The least prominent element is Zinc. The implant is an alloy having zinc in it. Its presence is unseen in the upcoming day. Figure 6.2 summarises the elements present on the magnesium alloy implant. (Zhang et al., 2009) *in vivo* studies mention P, C, Ca, O, and Mg in an *in vivo* Magnesium implant analysis.

6.3 Optical medium properties

The presence of gas bubbles can influence the optical path it passes. Literature (Deni Noviana a, 2016) shows the presence of hydrogen gas bubbles formed in a study of the survival rate of rats. Figure 6.3, taken from the same articles, mentions that day 5 has the

maximum size for these gas bubbles in the implantation period (Deni Noviana a, 2016, p. 11). It is interesting that *in vivo* experiments also have changes in the optical spectrum that varies with time. It is an indication of biological changes *in vivo* due to magnesium implantation. It supports the trend that is the center of this work, and hydrogen gases contribute to changes near the interface that shares the difference in optical spectrum and other biological changes at the site. It is exciting to understand that the OsloMet probe responds to the changes internally, giving a varied optical spectrum when collected from the left or right femur. It follows the observations of Deni Noviana in figure 6.3 B, which shows the changes in the gas cavities at different rat parts.

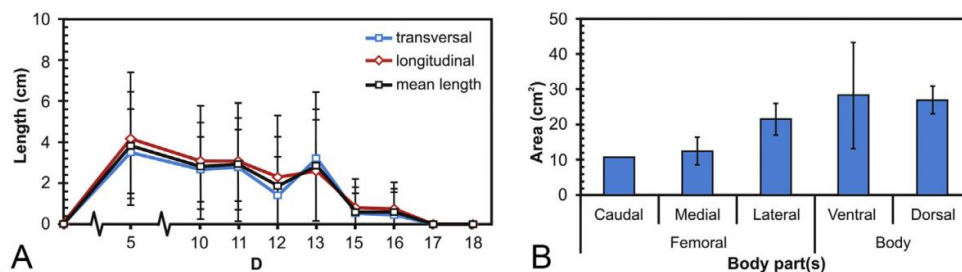


Figure 6. 3 (A) Gas cavity size evolution throughout the implantation period; and (B) gas cavity size at different rat parts. (Deni Noviana a, 2016, p. 11).

Note: This image is from (Deni Noviana a, 2016). Published under Creative Commons Attribution-Non Commercial-No Derivatives License (CC BY NC ND)

6.4 *In vitro* Vs *In vivo*

6.4.1 *In vitro* DMEM experiment

The pH variations for biodegradable and non-biodegradable implants in figure 3.7 from *in vitro* experiments highlight an initial rise in the pH when an implant material is in contact with DMEM. Biodegradable Mg has a higher pH variation than non-biodegradable Ti implants. It is due to higher concentrations of magnesium ions from magnesium-based implants that will interfere chemically with the salt ions (Willumeit-Römer, 2019, p. 1448) in the surrounding DMEM medium. The *in vitro* experiments suggest that the changes in pH are critical in the initial days, especially from the initial week. The *in vitro* experiment's connection can also be compared with the *in vivo* optical information. PCA analysis shows the feasibility of grouping optical data based on different days.

6.4.2 *In vivo* experiments

At present, medical practitioners use costly scans to evaluate the progress of implants, making the patient's life more complicated after the implant surgery (Hassan, Grasso, et al., 2021). Hence an optical approach that is less costly and patient-friendly can be of great interest. In the *in vitro* experiment, this trend, especially in magnesium alloy implants, is fascinating. There is a tendency to shift toward alkalosis that can impair surgery progress. Days soon after the implant are crucial and draw the need for medical attention and diagnosis if there is any deviation in expected progression.

Physiologic pH usually refers to the pH value of blood. In (Svorc & Petrášová, 2018), a table author compares blood pH in rats in different literature, highlighting around 7.4 as nominal. However, pH is local in a living body and varies slightly. The normal pH of skin surface for humans is slightly acidic (4.1 to 5.8), so it is different for mammals, as highlighted (Proksch, 2018). The pH of the young mouse is 5.4 and can rise to 5.9 for aged mouse skin. The trends in the pH graph for the *in vitro* experiment happen in living tissues as the *in vivo* implant interacts with water in the tissues. Nevertheless, the body's ability to naturally balance the body parameters shall suppress pH changes and maintain pH homeostasis. Blood has pH buffers such as hemoglobin and albumin that helps to maintain optimal balance in a living animal (Aoi & Marunaka, 2014). Post-surgery, the rise in pH near magnesium implant is due to the release of OH⁻ ions as it reacts with water (Jin et al., 2020). As the body starts to heal, there is a tendency of increased blood flow near the wound (Papazoglou et al., 2006). Thus, the tissues and implant interface undergo lots of changes that give functional (like metabolic changes) and structural (like surface changes) due to the magnesium implant inside the body.

6.4.3 Special case study from *in vivo* : Unhealthy and Died Rats

The spectrum from day 0 (the same day after surgery) and the third day of surgery in the exploratory model suggest maximum biochemical changes in the rats. The time with maximum optical changes can be related to the changes in local pH and higher concentrations of magnesium ions that will interfere chemically with salts in animal body

fluid. On day 0, there is damage to tissues locally near the interface as part of the surgery. As the wound starts to heal, higher blood flow perfusion near the surgery increases the blood flow. Thus there is an increase in chemicals (Mg^{2+} , Ca^{2+} , Cl^- , HCO_3^- , HPO_4^{2-}) that are present in the blood as detailed in table 4 of reference (Chakraborty Banerjee et al., 2019). These ions are the backbone of the leading chemical reactions near the implant. In these chemical reactions, changes are leading to variation in animal dehydration. It confirms the observations of unhealthy rats and dead rats from an exploratory model that week of post-surgery is critical concerning wound healing that decides the progress of surgery. Rat 70 died on day 3. Optical data gathered from rat 71 (unhealthy rat) and rat 70 (dead rat) was on day 3, far away from the optical data of healthy rats.

(Papazoglou et al., 2006, p. 1053 figure 10) Experimental results on healthy and unhealthy rats (diabetic rats) explain that the absorption coefficient of the optical spectrum is stable over time (5th day till 25th day). Strong absorption of NIR light relative to wound healing in healthy rats at 685nm gives information about deoxygenated hemoglobin near the surgical area. Papazoglou also suggests the possibility of tissue dehydration near the wound due to the in vivo implant. Higher ranges near 900nm to 1000 nm are regions of water absorption.

In PCA analysis, unhealthy rats' data points are away from the two healthy rats, shown in figure 5.11. Hence these two rats are used as a reference in this pilot study to compare unhealthy ones. Rat71 survived, but its optical spectra were not the same rats 64 or 65. Figure 5.15 in wavelengths below 850nm indicates the combined effect of variation in hemoglobin & cellular metabolism near the wound resulted in negative results for rat70 and 71. The rat 70 that died on day 3 indicates an abnormality in the optical spectra. The dead rat has dehydration-related concerns as the peak changes are much more significant than after 900nm. It can be a triggering cause for its death.

Papazoglou mentions that wound size in cm^2 is closely related to the healthiness of the rat. The author, in table 1, highlights that wound size reduces drastically from the fifth day to the tenth day and continues till the 15th day, after which it is almost the same. The in vivo experiment compared the first two weeks of surgical progression, where rat71 could survive but had different spectra. Studies show that it had rashes on its skin. Thus from in vivo, the

survived rat, r71, had issues in wound healing and was at a slower phase than other rats. Positively, researchers remember that the rashes were healing with time. Considering the thoughts of (Jayachandran et al., 2016) that optical data depends on local tissue, we conclude that optical changes in spectra collected from rat 71 are due to healing delays. Thus, the two unique case study of rats helps to answer the article's research question with proof.

6.5 Strength and weakness of the model

The weakness of this exploratory model is that the “prediction” of the changes for *in vitro* or progress of surgery for *in vivo* experiments based on the day was impossible with limited samples. A multiclass classification model based on the day was the target set. A prediction model can be built only with additional samples. Samples are also needed to validate model performance. Test samples had to be entirely new samples that were not part of the modeling and validation samples. Test samples need an optical spectrum with maximum varied health conditions to capture differences. For the PCA model, the sample size needs to be multiple of the variable number (Hua et al., 2004). Thus additional studies can be done with the reduced number of wavelengths.

The thesis is a pilot study at OsloMet that helps identify the future possibilities of the developed probe. The work identifies the feasibility of using optical spectrum to capture changes near the interface from *in vitro* and *in vivo* experiments and highlights a similar trend. The strength of the work is the possibility of evaluating surgical progression from the optical spectrum non-invasively without destroying the tissues. The reactions introduce functional and structural changes near its vicinity. These observations are in sink with other studies in the area. The *in vivo* experiment results help to make the study realistic.

7. Challenges & future scope

The research purpose is predefined, but not the paths to achieve it. In phase 1, the research plan starts with facilities and resources at OsloMet and the University of Oslo, the two universities under the umbrella of MgSafe in Norway, keeping in mind the challenges in the year 2021 with deep concerns about the pandemic's limitations.

7.1 Timeline for thesis

Close monitoring of the situation, openness to grab all opportunities, and continuous effort helped cover more than initially planned. The final updated timeline of this research work at three different phases is in table 2

Table 2 Timeline with highlighting different areas covered across semesters

SEM 2 (Q1) JAN 2021		SEM 2 (Q2)	SEM 3 (Q3) AUG 2021		SEM 3 (Q4)	SEM 4 (Q5) JAN 2022		SEM 4 (Q6)
Learn different Spectroscopy asurements		Me	Learn the Orange3 Software	Implement the workflow in Orange s/w	Learn Python for PCA	Prediction model		
Study of Mg - Tissue Interface	Study of Probe Prototype		Learn about PCA	Work on prediction of (timepoint and pH)	Learn python for prediction	identify performance parameters		
Study on biomarkers	Dead Tissue experiment		use unscrambler to understand PCA from the existing dataset	Analyze Gel tissue expt. in Orange s/w	PCA for in-vitro studies	PCA for <i>in vivo</i> studies		
Study Unscrambler software	Gel tissue-based expt.			Analyze Gel tissue expt. in Orange s/w	Probe studies to generate pulses	Biochemistry studies		
Literature survey	Draft phase 1 report		Prepare study Notes	Draft progress report	Prepare study Notes	Final report & research article		

7.2 Challenges Faced

In this section, the main challenges are mentioned. Later in this chapter, I summarise a few areas that I had worked on but excluded from the main discussions as it is incomplete with available data. This report includes these details so that future researchers can learn from my mistakes. I have also detailed some approaches for modeling.

7.2.1 Pandemic challenges

In phase 1, while deciding on the problem statement and analysis, there were quite many uncertainties related to the pandemic. Animal studies by MgSafe researchers were in the planning phase and could not finalize dates due to regulation changes. Hence the animal studies were excluded for fear of an extended travel ban outside Norway. Fortunately, between the first and second wave, the researchers were able to meet, and hence this thesis became a realistic study with *in vivo* experiments. My problem statement and research questions must also be modified as work progresses.

7.2.2 Concerns in the software platform

In the initial stage, data analysis was using UnscramblerX software. Due to some reasons, there was a need to shift to another open-source platform. Data analysis software Orange3 was easy to use for primary observations. However, I faced a few challenges in proceeding with the same tool. Each building block in the software is known as a widget. It helps to build the workflow as needed by the user. As the software uses the inbuilt widgets, its modification options limit its features. Some widgets, especially preprocess and model widgets, have default settings to normalize the data as it passes through. It loses data control as it passes from one widget to another, making it difficult to conclude the observations. Evaluating the performance parameters was not easy. Also, there were some technical issues due to which widgets received invalid or null data as it passed from one widget to another. Finally, there were a few difficulties while developing a pipeline for the data analysis. Hence I finally used sklearn packages that used open-source python programming to perform data analysis. Though python was new, any other programming

language background and understanding the requirements can help the beginner as there are numerous online contributions. I have mentioned some useful links in Appendix B's footnotes and helpful code snippets.

7.2.3 Issues related to a prediction based model

While performing the DMEM *in vitro* lab experiments, we took 10 measurements from a particular sample with the assumption of 30 data points as there were 3 samples for a particular implant type. Unfortunately, working on these piolet studies reveals that ten samples collected within a short time on a particular day have overlapping points in the PC1-PC2 plain. Thus these 30 data points got reduced to 3 datapoints clusters (one cluster per sample). These unexpected limitations blocked the prediction model as it needed many samples.

On day 5, three different sample clusters were spread in PCA plain, influencing 96.9% of PC1. There is a need to remove outliers or inconsistent data to improve the PC1. Unfortunately, due to limited samples, removing one sample is difficult. Moreover, it is not possible to understand the trend with 2 samples. Getting additional rat samples for *in vivo* data was not easy, as there was much preparation for that experiment. By the time the issue was identified, there was only two weeks gap that wasn't sufficient to process it due to lots of preparation involved in the task.

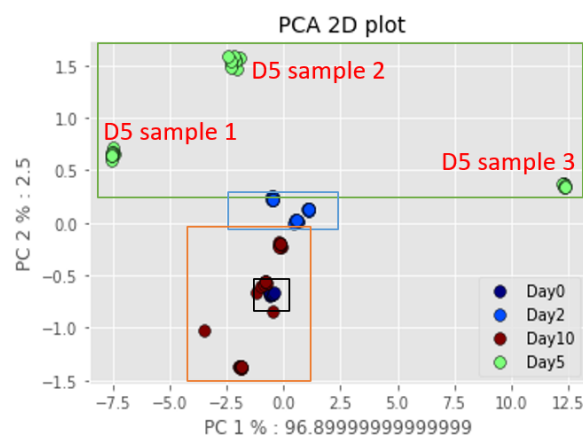


Figure 7. 1 *In vitro* experiment based on PCA highlighting the samples of day 5

I had tried on prediction from *in vitro* data based on the day as the target with available data. Unfortunately, proceeding with the available data was not the best approach for the thesis. While exploring the modeling aspects, there was a surprising observation. It is

possible to have excellent performance in the prediction model based on the day if the model and test have entirely different data points taken from the same samples. That means of the 10 measurements from a sample, the model uses measurements 1,3,5,6,7,9,10, and validation uses 2,4,8 measurements. It makes model data different from testing or validation data. However, it is not a dependable model, even with improved performance parameters. It was interesting to note that the performance (accuracy) of the KNN classifier model was cent percent. However, I concluded it was a cheat model due to two reasons. Firstly it is not a realistic approach. In an actual situation, model generation and its validation is with the help of data from specific samples, and testing samples have to be entirely new samples (patients). Then only testing becomes complete. It was my first observation. Again, PCA analysis shows that most samples have a clustered nature (Figure 7.1). KNN that uses K nearest neighbor can easily group the test points from a particular sample in this experiment. It was the reason for the high value for accuracy. A new attempt is to use sample 1,2 for modeling and validation. Testing with the last third sample was the next attempt. Unfortunately, the modeling work was blocked as there are no samples to validate the model. But it is the correct approach to be followed as test patients are always new. Were these studies advantageous?

Studies are never a loss, and they helped me learn many new concepts in machine learning and learn new software platforms. My notes can be helpful for budding researchers to plan in the future — the next section details more of my notes for them. The main idea of seeing the trend concerning the day arrived from these studies: the thesis's main flow.

7.3 Future Directions for researchers

7.3.1 Data collection

So the first main conclusion of this discussion is that make sure to have different and sufficient samples for modeling, validation, and testing. Either, 80% :20% or 70%: 30% is the modeling and validation data ratio. Also, there needs to be a minimum of 3 samples understanding the trend in the model. There are always chances of unforeseen experimental error; hence an additional sample is preferred. Then, validation needs at least two samples. Testing unknown samples needs to be a separate dataset different from modeling and

validation samples. It is interesting to perform testing on at least one similar and non-similar test sample to evaluate its performance. Thus a minimum of "ten samples per implant type" is recommended. Having more samples (Hua et al., 2004) for further studies when performing prediction-based models is helpful. A thumb rule says the number of samples needs to be multiple of the number of variables used in PCA. That calls for reducing the variables (wavelengths) to the most promising range like 700 to 800nm and 950 to 975nm.

To use a classifier-based prediction model to predict the progress of surgery based on the day. There need to be sufficient data points for more days. There is a need to recheck the extent of overlapping days when more days are part of the analysis. Frequent data collection in the first week slowly increases the gap with time and can be more creative in modeling. A healthy rat gets its wound healing stable in about 2 weeks. But the implant degrades slowly with time. Hence it is recommended to take non-systematic data collection for at least a month. It is challenging for *in vivo* experiments to have systematic data collection due to the test procedure guidelines to take care of animals' well-being. Hence if resources are available, it shall be effective to have even rat groups and odd rat groups so that it is possible to get optical data for all the days in the first week.

7.3.2 Prediction model based on classification approach

To create a predictive model, split the available data into model and validation data, usually in the 80: 20 percentage ratio (X) and target (Y), assuming separate data samples to test this prepared model. Then based on the type of binary or multiclass classifier, create the model using the labeled model data X and model target Y. Classifier studies the given input and generates the model. Validate the model with the help of each sample X from validation data. It generates a prediction based on input X to the classifier model. It can be compared with the expected target of the sample to evaluate if the prediction was right or wrong. The confusion matrix is the table form of a summary of the prediction results.

Among different classifiers, KNN is the simplest one that works well with these optical datasets due to the clustered points in the PCA plain. KNN predicts the unknown sample based on the nearest neighbors 'K' number. Model votes for the highest group of nearest neighbors and classifies into that group. How to get the best k value for the model? To get

the best K value, perform initial testing. KNN model is to be created by iterating for different values of K in the base model. Using the validation data samples, test the model performance for each iteration by getting the mean square error. Record the values in an error array. Plot this error array containing the mean square error for different K values. The k with the lowest k is identified for the final primary model to get the highest accuracy.

Performance parameters: Confusion matrix

The confusion matrix applies well to binary class classifiers. True positive (TP) are those predictions that are predicted positive or yes and were positive themselves. Likewise, true negative (TN) values are negative (or no) and predicted the same. False Positive (FP) counts falsely positive records, which means they are negative but predicted positive or Yes. False-negative (FN) is its opposite. The table below is a typical binary class confusion matrix that predicts healthy/unhealthy.

With samples like DMEM datasets, it is possible to have three (day2, 5, 10) multiclass classifiers, and a confusion matrix is sufficient to define the performance. Unlike the binary class-based confusion matrix, the multiclass obtains the values for each criterion. For the *In vitro* experiment, day 2, day 5, and day 10 were the target for prediction. So a new sample is also expected to give prediction based on the reaction progression for that day.

Due to the lack of samples, we could not perform the necessary validation process of the model that uses samples 1 and 2. The confusion matrix and its calculations use sample 3 as validation data with 10 data samples from each time point. Figure 7.2 (b) has green circles that are the actual positive values in the confusion matrix, meaning it was criteria_a and predicted as criteria_a itself. At the same time, the orange circles represent the False positive which means that they actually belong to criteria_a but are falsely predicted as criteria_b. With these values, it is possible to obtain the performance parameters of a prediction model in terms of precision, recall, and F1 score concerning each criterion and model accuracy, as seen in the classification report concerning the model. Generation of classification report is possible from an already defined classifier. We need to pass the actual values and predicted values to the function.

It is possible to model KNN multiclass classifier in python code with the help of the KNN classifier package. The classification report lists the performance parameters. The recall is also known as the sensitivity of the model. Parameter's precision gives the possibility to

predict that particular criterion. F1 score is a combined parameter. In general, accuracy helps explain the model performance most easily.

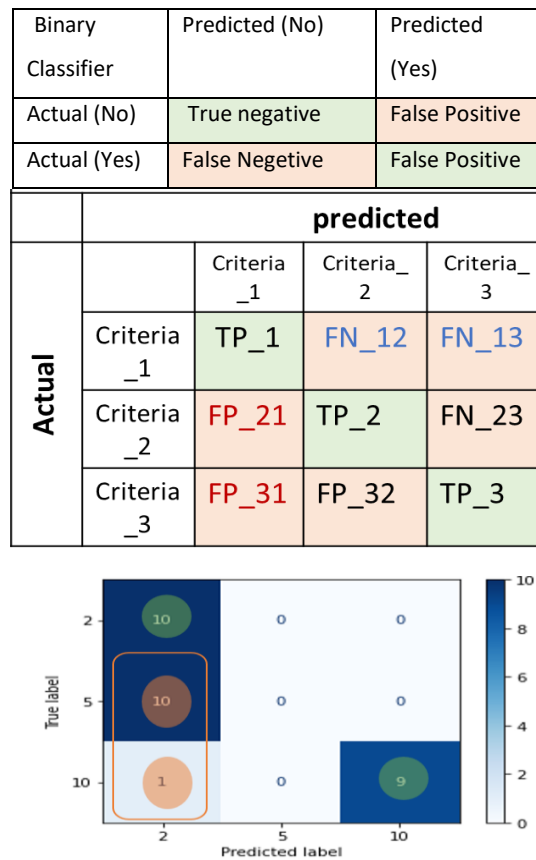


Figure 7. 2 (a) Binary classifier (b) Multi class Confusion Matrix: a general representation (c) as obtained from DMEM datasets for the Mg alloy model

$$precision_{criteria_1} = \frac{TP_1}{TP_1+FP_{21}+FP_{31}} \text{ for example; } precision_{day2} = \frac{10}{10+10+1} = 0.4762$$

$$Recall_{criteria_1} = \frac{TP_1}{TP_1+FN_{12}+FN_{13}} ; Recall_{day2} = \frac{10}{10+0+0} = 1$$

$$F1_{criteria_1} = \frac{2*TP_1}{2*TP_1+(FP_{21}+FP_{31})+(FN_{12}+FN_{13})} , F1_{criteria_1} = \frac{2*10}{2*10+(11)+(0)} = 0.645$$

$$Accuracy \text{ of model} = \frac{\text{All correct predictions}}{\text{Total number}} = \frac{TP_1+TP_2+TP_3}{(TP_1+TP_2+TP_3)+(FP_{21}+FP_{31}+FP_{32})+(FN_{12}+FN_{13}+FN_{23})} = 0.63333$$

```

KNN classification_report (sample 3 as prediction sample)
K=48

```

	precision	recall	f1-score	support
2	0.48	1.00	0.65	10
5	0.00	0.00	0.00	10
10	1.00	0.90	0.95	10
accuracy			0.63	30
macro avg	0.49	0.63	0.53	30
weighted avg	0.49	0.63	0.53	30

Figure 6. 4 Performance parameter of classifier model (classification report)

However, if data points are from more days in future studies, the classes or groups in the model increase. In such multiclass classifiers, as the number of classes increases, instead of a confusion matrix, AUC-based results are more helpful. The basic codes helpful for coding are in appendix B.

7.3.3 Probe studies

Present studies are done using a continuous wave of light. If we can control the light intensity, there is a possibility of uncovering more domains. However, it has the complexity of overlap of light. The second suggestion is to develop the idea as a medical device. The present studies show that those specific wavelengths contribute more to the optical dataset. Thus there is the possibility of designing optical probes specific to wavelengths of interest. It helps to make a device by removing the spectrometer. Then the device can be cost-effective. However, there is a need to identify how to design the data collection and preprocessing. It can be interesting to compare and study the optical spectra and their influence on different types of magnesium alloy. How does it affect the pH? Which alloy responds with a more significant response to the optical probe?

7.4 Future scope

The trends from the *in vivo* and *in vitro* experiments highlight the possibility of separating the difference in implant interface concerning changes in the medium through its passes. The PCA studies show that the data points cluster extensively. Hence there is a possibility to develop a simple KNN multi-class classifier model to predict surgery progress. *In vivo*

experiments suggest developing this model with healthy rats that define the region for each day. In the *in vivo* dataset, we see regions that separate the day. Interestingly, PC1-PC2 and PC2-PC3 separate the day-based changes. It is interesting to note that PC1-PC2 / PC2-PC3 can develop a healthy rats-based PCA model with a sufficiently large number of samples in the future to confirm the areas it covers.

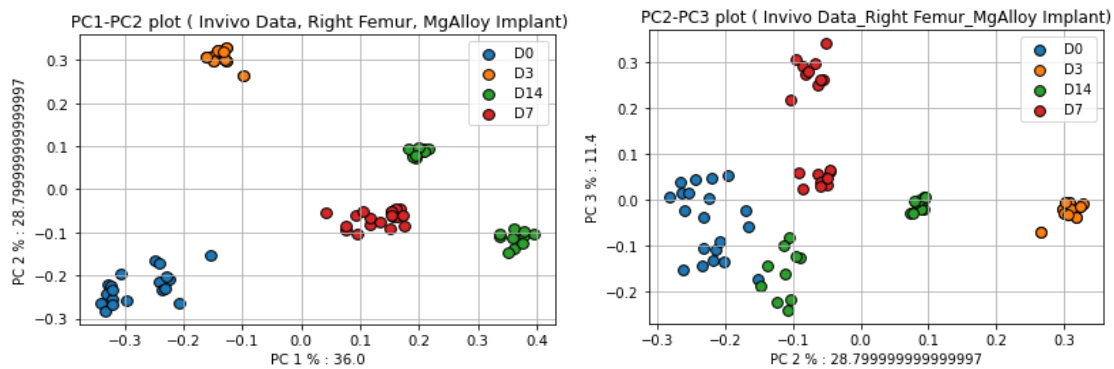


Figure 7. 3 PCA of healthy rats r64 and r65 (a) PC1 PC2 plot (b) PC2-PC3 plot

The unknown sample collected from a particular day in a new animal expects to be close to that day. If it separates from the healthy cluster (like the rat with rashes after surgery / dead rat), it is an indication that the changes *in vivo* are not in the expected pattern, and there is a need for medical diagnosis.

New cells replace the damaged cells near the implant, where surgery destroys the nearby cells and tissues. As the wound heals, blood flow increases near the injury at the interface. Thus along with structural, there are significant functional changes at the implant interface. To sum up, comparing *in vivo* datasets is a promising way to compare the observations of *in vitro* datasets.

This research opens up that the device can be modeled later in upcoming years to connect the optical spectrum to other physiological parameters like the oxygen level of the animal, metabolic parameters like cytochrome C oxidase, hemoglobin in the blood, and blood the information of the progress of surgery of the magnesium Implant (Rosen et al., 2002). It can be the supportive information to decide the necessary steps to help the subjects (animal models) cope with the situations. If the health conditions are progressing with changes in day points as expected, an alert message on good health can inspire the medical researchers to monitor the animals. Timely help to the animals can help to reduce the unknown stress.

From a medical perspective, I would recommend closer medical attention for patients from the surgery for the first week, as it is the main day that can decide the progress of an implant. From the trend of the pH curve, we can see that variation in pH is getting stabilized after day 5 for a magnesium alloy implant. Hence, *in vivo* implants shift towards alkalosis due to the alloy reactions being balanced or neutralized within the body. If the body cannot maintain the local pH near the interface, there is every chance that the cells and tissues get damaged.

It takes months for the bone to heal. Studies show that initial days are critical even for magnesium alloy-based implants. With such a user-friendly device connected to Wifi, facilities should enable patients to rest at home with self-diagnosis or remote diagnosis via a medical practitioner. In case of any difference in expected changes, the patient needs to travel to the hospital. It helps to improve the QALY of affected patients. Biodegradable implants shall help to avoid the need for a second surgery.

Thus the future of optical spectrum-based medical diagnosis for predicting the progress of magnesium implant-based surgery has a bright future.

Conclusion

An exploratory study to understand the changes at the magnesium implant interface is the core of this work. *In vitro* DMEM-based experiment helps to identify the trend. The possibility of separating days is intriguing in the *in vivo* studies. Deciding the outliers is challenging for *in vitro* with drastic dependency on PC1, especially from day five samples. The *in vivo* studies were made from the right femur alone to make the model more reliable. The pH curve suggests that till day 5, numerous chemical changes happened in the interface. The biochemical analysis of magnesium implant explores the internal changes near the interface. The analysis of *in vivo* datasets gave the observations meaningful thoughts to compare healthy with unhealthy rats. Lab experiments and literature suggest day 5 to have maximum influence. For magnesium alloy implants, local pH is a biomarker that strongly correlates to the changes near the implant interface. *In vivo*, optical spectra are complex due to biological chromophores. All the biochemical changes influence the optical spectrum and form specific expected changes on each post-surgery day. This thesis examined two particular cases of rats and confirmed that it is possible to separate unhealthy rats from healthy ones optically. These observations confirm the feasibility of optically predicting implant surgery's progress due to its interaction at the interface. Additional experiments help learn more about the optical probe and ways to improve it.

As bones need time to heal, the patients need medical support for an extended period.

Sometimes it takes months before the implant degrades completely. Simple self-diagnosis models that compare the optical data based on the model with healthy optical data on different days from the day of surgery can help them relate their health conditions.

Additional information on oxygen saturation, hemoglobin, and water hydration can also help predict a need to go to the hospital for a medical checkup. After the first few days of hospitalization, patients can rest in their homes with a supportive medical device. It helps to improve the life quality. The future of optical spectrum-based evaluation of progress for magnesium implants is bright. This experimental study shows that hydrogen gas, pH, water, hemoglobin, and cell metabolism changes collectively give a safe expected direction of reaction that supports wound healing post-surgery. It is specific to the day. Thus, it can support patients as an optical health care device with further developments in the future.

Reference List

- Aoi, W., & Marunaka, Y. (2014). Importance of pH Homeostasis in Metabolic Health and Diseases: Crucial Role of Membrane Proton Transport. *BioMed Research International*, 2014, 1-8. <https://doi.org/10.1155/2014/598986>
- Bairagi, D., & Mandal, S. (2021). A comprehensive review on biocompatible Mg-based alloys as temporary orthopaedic implants: Current status, challenges, and future prospects. *Journal of Magnesium and Alloys*. <https://doi.org/10.1016/j.jma.2021.09.005>
- Borgström, F., Karlsson, L., Ortsäter, G., Norton, N., Halbout, P., Cooper, C., Lorentzon, M., McCloskey, E. V., Harvey, N. C., Javaid, M. K., & Kanis, J. A. (2020). Fragility fractures in Europe: burden, management and opportunities. *Archives of Osteoporosis*, 15(1). <https://doi.org/10.1007/s11657-020-0706-y>
- Castiglioni, S., Cazzaniga, A., Albisetti, W., & Maier, J. (2013). Magnesium and Osteoporosis: Current State of Knowledge and Future Research Directions. *Nutrients*, 5(8), 3022-3033. <https://doi.org/10.3390/nu5083022>
- Chakraborty Banerjee, P., Al-Saadi, S., Choudhary, L., Harandi, S. E., & Singh, R. (2019). Magnesium Implants: Prospects and Challenges. *Materials*, 12(1), 136. <https://doi.org/10.3390/ma12010136>
- Deni Noviana a, D. P., Mokhamad Fakhrol Ulum, Hendra Hermawan. (2016). The effect of hydrogen gas evolution of magnesium implant on the postimplantation mortality of rats. *Journal of Orthopaedic Translation*, 5, 9-15. <https://doi.org/https://doi.org/10.1016/j.jot.2015.08.003>
- Ding, W. (2016). Opportunities and challenges for the biodegradable magnesium alloys as next-generation biomaterials. *Regenerative Biomaterials*, 3(2), 79-86. <https://doi.org/10.1093/rb/rbw003>
- Fan, Y., Liao, Y., & Cheng, F. (2018). Predicting of intramuscular fat content in pork using near infrared spectroscopy and multivariate analysis. *International Journal of Food Properties*, 21(1), 1180-1189. <https://doi.org/10.1080/10942912.2018.1460606>
- Hassan, H. W., Grasso, V., Korostynska, O., Khan, H., Jose, J., & Mirtaheri, P. (2021). An overview of assessment tools for determination of biological Magnesium implant degradation. *Medical Engineering & Physics*, 93, 49-58. <https://doi.org/10.1016/j.medengphy.2021.05.016>
- Hassan, H. W., Mathew, A., Khan, H., Korostynska, O., & Mirtaheri, P. (2021). *Feasibility Study of Multi-Wavelength Optical Probe to Analyze Magnesium Implant Degradation Effects*.
- Hua, J., Xiong, Z., Lowey, J., Suh, E., & Dougherty, E. R. (2004). Optimal number of features as a function of sample size for various classification rules. *Bioinformatics*, 21(8), 1509-1515. <https://doi.org/10.1093/bioinformatics/bti171>
- Jayachandran, M., Rodriguez, S., Solis, E., Lei, J., & Godavarty, A. (2016). Critical Review of Noninvasive Optical Technologies for Wound Imaging. *Advances in Wound Care*, 5(8), 349-359. <https://doi.org/10.1089/wound.2015.0678>
- Jin, S., Zhang, D., Lu, X., Zhang, Y., Tan, L., Liu, Y., & Wang, Q. (2020). Mechanical properties, biodegradability and cytocompatibility of biodegradable Mg-Zn-Zr-Nd/Y alloys. *Journal of Materials Science & Technology*, 47. <https://doi.org/10.1016/j.jmst.2020.02.017>

- Kabir, H., Munir, K., Wen, C., & Li, Y. (2021). Recent research and progress of biodegradable zinc alloys and composites for biomedical applications: Biomechanical and biocorrosion perspectives. *Bioactive Materials*, 6(3), 836-879. <https://doi.org/10.1016/j.bioactmat.2020.09.013>
- Kim, T., See, C. W., Li, X., & Zhu, D. (2020). Orthopedic implants and devices for bone fractures and defects: Past, present and perspective. *Engineered Regeneration*, 1, 6-18. <https://doi.org/10.1016/j.engreg.2020.05.003>
- Kumar, R., & Katyal, P. (2021). Effects of alloying elements on performance of biodegradable magnesium alloy. *Materials Today: Proceedings*. <https://doi.org/10.1016/j.matpr.2021.08.233>
- Liu, C., Ren, Z., Xu, Y., Pang, S., Zhao, X., & Zhao, Y. (2018). Biodegradable Magnesium Alloys Developed as Bone Repair Materials: A Review. *Scanning*, 2018, 1-15. <https://doi.org/10.1155/2018/9216314>
- Luo, S., Pal, D., Shah, S. J., Kwatra, D., Paturi, K. D., & Mitra, A. K. (2010). Effect of HEPES Buffer on the Uptake and Transport of P-Glycoprotein Substrates and Large Neutral Amino Acids. *Molecular Pharmaceutics*, 7(2), 412-420. <https://doi.org/10.1021/mp900193e>
- Mathew, A., Hassan, H. W., Mirtaheri, P., & Korostynska, O. (2021). Feasibility of Using NIR Spectroscopy in Automated Meat Cutting. European Robotics Forum 2021. https://www.robotchur.eu/wp-content/uploads/2021/05/ERF2021_proceedings_final.pdf
- Papazoglou, E., Weingarten, M., Zubkov, L., Zhu, L., Tyagi, S. D., & Pourrezaei, K. (2006). Optical Properties of Wounds: Diabetic Versus Healthy Tissue. *IEEE transactions on bio-medical engineering*, 53, 1047-1055. <https://doi.org/10.1109/TBME.2006.873541>
- Prieto, N., Pawluczyk, O., Dugan, M. E. R., & Aalhus, J. L. (2017). A Review of the Principles and Applications of Near-Infrared Spectroscopy to Characterize Meat, Fat, and Meat Products. *Applied Spectroscopy*, 71(7), 1403-1426. <https://doi.org/10.1177/0003702817709299>
- Proksch, E. (2018). pH in nature, humans and skin. *The Journal of Dermatology*, 45(9), 1044-1052. <https://doi.org/10.1111/1346-8138.14489>
- Radha, R., & Sreekanth, D. (2017). Insight of magnesium alloys and composites for orthopedic implant applications – a review. *Journal of Magnesium and Alloys*, 5(3), 286-312. <https://doi.org/https://doi.org/10.1016/j.jma.2017.08.003>
- Rosen, N. A., Charash, W. E., & Hirsch, E. F. (2002). Near-Infrared Spectrometric Determination of Blood pH. *Journal of Surgical Research*, 106(2), 282-286. <https://doi.org/10.1006/jsre.2002.6377>
- Sakata, Y., Abajian, M., Ripple, M. O., & Springett, R. (2012). Measurement of the oxidation state of mitochondrial cytochrome c from the neocortex of the mammalian brain. *Biomedical optics express*, 3(8), 1933-1946. <https://doi.org/10.1364/BOE.3.001933>
- Sun, J. (1997). Statistical analysis of NIR data: data pretreatment. *Journal of Chemometrics*, 11(6), 525-532. [https://doi.org/https://doi.org/10.1002/\(SICI\)1099-128X\(199711/12\)11:6<525::AID-CEM489>3.0.CO;2-G](https://doi.org/https://doi.org/10.1002/(SICI)1099-128X(199711/12)11:6<525::AID-CEM489>3.0.CO;2-G)
- Svorc, P., & Petrášová, D. (2018). Arterial pH and Blood Gas Values in Rats Under Three Types of General Anesthesia: a Chronobiological Study. *Physiological research*, 67. <https://doi.org/10.33549/physiolres.933692>

- Taber, K. H., Hillman, E. M. C., & Hurley, R. A. (2010). Optical Imaging: A New Window to the Adult Brain. *The Journal of Neuropsychiatry and Clinical Neurosciences*, 22(4), iv-iv. <https://doi.org/10.1176/jnp.2010.22.4.iv>
- Tsakiris, V., Tardei, C., & Clicinschi, F. M. (2021). Biodegradable Mg alloys for orthopedic implants – A review. *Journal of Magnesium and Alloys*. <https://doi.org/10.1016/j.jma.2021.06.024>
- Wang, J. L., Xu, J. K., Hopkins, C., Chow, D. H. K., & Qin, L. (2020). Biodegradable Magnesium-Based Implants in Orthopedics—A General Review and Perspectives. *Advanced Science*, 7(8), 1902443. <https://doi.org/10.1002/adv.201902443>
- Westad, F., Hersleth, M., Lea, P., & Martens, H. (2003). Variable selection in PCA in sensory descriptive and consumer data. *Food Quality and Preference*, 14(5), 463-472. [https://doi.org/https://doi.org/10.1016/S0950-3293\(03\)00015-6](https://doi.org/https://doi.org/10.1016/S0950-3293(03)00015-6)
- Willumeit-Römer, R. (2019). The Interface Between Degradable Mg and Tissue. *JOM*, 71(4), 1447-1455. <https://doi.org/10.1007/s11837-019-03368-0>
- Zhang, E., Xu, L., Yu, G., Pan, F., & Yang, K. (2009). In vivo evaluation of biodegradable magnesium alloy bone implant in the first 6 months implantation. *Journal of Biomedical Materials Research Part A*, 90A(3), 882-893. <https://doi.org/https://doi.org/10.1002/jbm.a.32132>

Appendices

Appendix A: Additional Achievement

A1: Main author conference publication

Feasibility of Using NIR Spectroscopy in Automated Meat Cutting

Anna Mathew, Hafiz Wajahat Hassan, Peyman Mirtaheri*, Olga Korostynska**

MEK, TKD, Oslo Metropolitan University (OsloMet), and Norwegian University of Life Sciences (NMBU), Faculty of Science and Technology (REALTEK), Ås, Norway

OVERVIEW

- ✓ Optical methods @ Near InfraRed (NIR) spectroscopy.
- ✓ Feasibility of using NIR for real-time assessment of meat samples in automated meat cutting is assessed.
- ✓ Lab experiments to correlate fat and its thickness, muscle layers and bone of a fresh pork sample.
- ✓ Spectral analysis is widely used in meat industry.
- ✓ Improved design of a robust optical probe for this purpose is necessary.
- ✓ Used reflectance type NIR spectroscopy.
- ✓ Two different probe designs were tested & compared. Unscrambler X was used for analysis.
- ✓ spectrometer supported by Avantes software

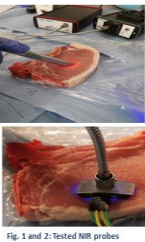


Fig. 1 and 2: Tested NIR probes

No.	Sampling thickness	Sample details of sample location
1	Fat 1.6cm	Fat (thick) position
2	Fat 8mm	Fat (close to 1 cm thick)
3	Fat 4mm	Fat/muscle boundary
4	Fat 2mm	Fat/muscle boundary
5	Fat 1mm	Fat/muscle boundary
6	Fat 0mm	muscle begins
7	Muscle 1.8cm position 1	Muscle (width position 1 of thickness 1.8 cm)
8	Muscle 1.8cm position 2	Muscle (width position 2)
9	Muscle 1.8cm position 3	Muscle (width position 3)
10	Bone side 1	hard bone structure side position
11	Bone side 2	hard bone structure side position

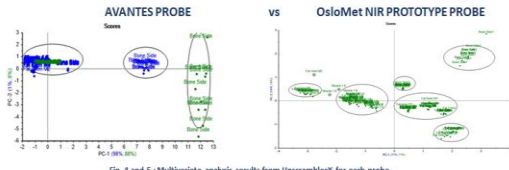


Fig. 4 and 5: Multivariate analysis results from UnscramblerX for each probe.

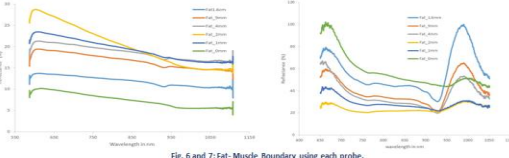


Fig. 6 and 7: Fat-Muscle Boundary using each probe.

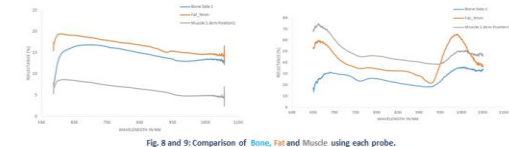


Fig. 8 and 9: Comparison of Bone, Fat and Muscle using each probe.

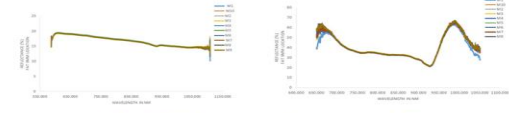


Fig. 10 and 11: Repeatability of probe based on 10 samples in one location, using 2 NIR probe.




Fig. 3: 11 different test points (Table gives further details)

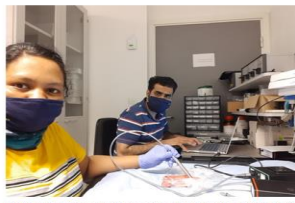


Fig. 12: Anna (Master student) and Wajahat (PhD candidate) collecting data in OsloMet lab using Avantes probe.

CONCLUSION

- ✓ Developed lab probe showed clear separation of all data with different component (with accuracy of 87 %).
- ✓ Prototype developed in OsloMet lab was able to respond with distinguishable peaks based on varying thickness.
- ✓ Highly repeatable readings & non-invasive in nature supports feasibility of using NIR spectroscopy in meat industry during automated cutting.

REFERENCES

[1] Y. Fan, Y. Liao, and F. Cheng, "Predicting intramuscular fat content in pork using near infrared spectroscopy and multivariate analysis," *International Journal of Food Properties*, vol. 21, no. 1, pp. 1180-1189, 2018, doi: 10.1080/10942912.2018.1469606.

[2] N. Pireto, O. Pawluczuk, M. E. R. Dagan, and J. L. Aalhus, "A Review of the Principles and Applications of Near Infrared Spectroscopy to Characterize Meat, Fat, and Meat Products," *Applied Spectroscopy*, vol. 71, no. 7, pp. 1403-1426, 2017, doi: 10.1177/0003702817099299.

ACKNOWLEDGEMENT

This work was supported by the EC H2020 project "RoBUTCHER" grant agreement No.871631 and MSCA-ITN-ETN "MgSafe" under the Marieklodowska-Curie grant agreement No 811226.

Contacts:

*peymanm@oslomet.no, **olga.korostynska@nmbu.no

Figure A. 1 Poster presented used for Conference presentation

Won Prize for Best Poster: In an online conference RoBUTCHER @ European Robotics Forum 2021⁴.

Anna Mathew, Hafiz Wajahat Hassan, Peyman Mirtaheri, and Olga Korostynska, "Feasibility of Using NIR Spectroscopy in Automated Meat Cutting" Proceedings of the Challenges in Automated Food Processing, European Robotics Forum (ERF 2021), ISBN 978-963-449-242-9, pp. 10-12, April 2021.




⁴ Link for details of the conference.



<https://www.nmbu.no/en/faculty/realtek/research/groups/roboticsandcontrol/news/node/42656>

A2: IEEE conference publication details (Co-author)

- *Title: Feasibility Study of Multi-Wavelength Optical Probe to Analyze Magnesium Implant Degradation Effects.*
- *Authors: Hafiz Wajahat Hassan, Anna Mathew, Haroon Khan, Olga Korostynska, Peyman Mirtaheeri.*
- (Hassan, Mathew, et al., 2021) available at <https://ieeexplore.ieee.org/document/9639741>
- *Conference details: Paper ID-1373, IEEE Sensor 2021.*

Poster used for presentation by the first author

Feasibility Study of Multi-Wavelength Optical Probe to Analyze Magnesium Implant Degradation Effects
 Hafiz Wajahat Hassan*, Anna Mathew, Haroon Khan, Olga Korostynska, Peyman Mirtaheeri

OVERVIEW

- ✓ Near-infrared spectroscopy (NIRS) can be applied for spectrographic analysis.
- ✓ Measurements on the implant-tissue interface for hydrogen gas formation as part of magnesium degradation is essential for interpreting the biodegradable Magnesium (Mg) based implants [1].
- ✓ Introduces novel NIR optical probe that can assess the state of Mg Implant's degradation when in contact with biological tissues.

TISSUE –MIMICKING PHANTOM (TMP)

- ✓ A tissue mimicking phantom (TMP) to mimic biological tissue's optical properties helps investigate changes in reflectance spectra due to bubble formation at the implant-tissue interface.
- ✓ Spectra taken from different TMP samples containing Mg and Titanium (Ti) disk are suitable for evaluating the implant's interaction.
- ✓ The results show that the reflection in TMP for samples containing Mg disks, confirms the presence of hydrogen bubbles around them.

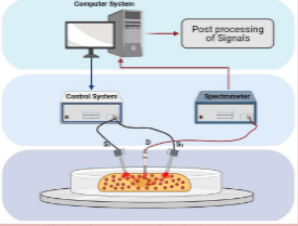


Fig. 1: Illustration of optical probe setup

MULTI WAVELENGTH OPTICAL PROBE

- ✓ Working Range from 600 nm to 1050 nm.
- ✓ Multi-distance optical probe with depth selectivity of 3mm and 4mm has shown to be an effective tool to monitor bubble effect on different samples.
- ✓ The designed optical probe's light sources are strictly compliant with threshold to ensure the operation safety.
- ✓ The optical probe target different sets of the region of interest (ROIs)

DEPTH VARIATION AND REFLECTANCE SPECTRA

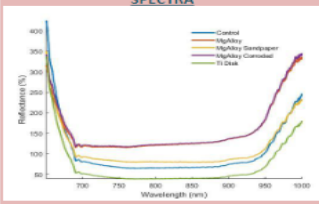


Fig. 2: Gel phantom's reflectance spectra (4-mm depth)

CONCLUSION

- ✓ Effect of bubble formation on reflectance spectra is studied using tissue-mimicking phantoms.
- ✓ Influence of bubbles at interface due to scattering in biological tissues is analyzed.
- ✓ Comparison of two different source-detector distances were separated 100% in PCA score plot.

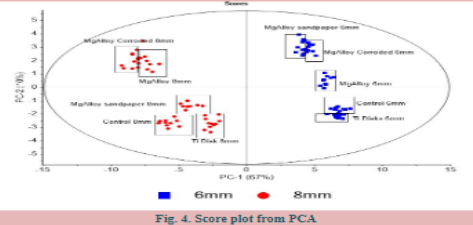


Fig. 4: Score plot from PCA

ACKNOWLEDGEMENT

- ✓ This publication is part of a project "Promoting patient safety by a novel combination of imaging technologies for biodegradable magnesium implants, MgSafe" that has received funding from the European Union's Horizon 2020 research and innovation program under the Marie Skłodowska-Curie grant agreement No 811226.

* Main Author : wajahat@oslomet.no

References

H. W. Hassan, V. Grasso, O. Korostynska, H. Khan, J. Jose, and P. Mirtaheeri, "An overview of assessment tools for determination of biological magnesium implant degradation," *Medical Engineering & Physics*, vol. 93, pp. 49–58, 2021.

Appendix B: Python code snippets

Min Max scaling

```
from sklearn.preprocessing import MinMaxScaler # import package
output_data= MinMaxScaler().fit_transform(input_data) # command
```

SNV (Standard Normal Variate) 5

approach : Divide each mean-centered spectrum by its own standard deviation: $X_{isnv} = (X_i - X_{imean})/\sigma$, data_snv has final data

```
input_data = np.asarray(input_data)
data_snv = np.zeros_like(input_data)
for i in range(data_snv.shape[0]):
    # Apply correction
    data_snv[i,:] = (scalingMin_max[i,:] - np.mean(scalingMin_max[i,:])) /
np.std(scalingMin_max[i,:])
```

First derivative applying a Savitzky-Golay filter

```
from scipy.signal import savgol_filter # import for filter
der1_output = savgol_filter(data_input , 25, polyorder = 5, deriv=1) # input data given &
set derivative needed
```

PCA

```
from sklearn import decomposition # import for PCA
```

```
pca_inputData = processedData # set the data whose PCA is to be calculated
n_components=10 # set number of components for PCA
data_after_pca = decomposition.PCA(10) # create object & set number of components for
PCA as 10
PCA_data = data_after_pca.fit(pca_inputData) # perform fit to finish PCA , then get
parameters
```

```
score_PCA =PCA_data.transform(pca_inputData) # Get PCA : Scores
loadings_pca =PCA_data.components_.T # fetch Loading values
explained_var_pca= PCA_data.explained_variance_ratio_ # explained variance for
percentage
cum_variance_pca = np.cumsum(np.round(explained_var_pca, decimals=3)) # calculate
cumulative variance
```

Splitting data to modeling and validation

```
from sklearn.model_selection import train_test_split
# X = scaled_data , y = target data , assign values and split based on test_size
```

⁵ <https://nirpyresearch.com/two-scatter-correction-techniques-nir-spectroscopy-python/>
<https://towardsdatascience.com/scatter-correction-and-outlier-detection-in-nir-spectroscopy-7ec924af668>

```
X_train, X_val, y_train, y_val = train_test_split(X,y,test_size=0.2 ,random_state=42,
stratify=y)
```

KNN (Classifier)⁶

```
from sklearn.neighbors import KNeighborsClassifier # import for KNNclassifier
from sklearn.metrics import mean_squared_error # For MSE error

error=[]
# get the error for different values of K
for k in range(1,50): # maximum value of K neighbours can be upto len(y_train)
    knn=KNeighborsClassifier(k)
    knn.fit(X_train,y_train) # feed the model DataX and target Y
    y_test_pred = knn.predict(X_val) # send the new samples that are not used for modeling
    error.append(mean_squared_error(y_val,y_test_pred ))
# Plot error curve and get the best K correpsponding to lowest error . Setup a knn classifier
with k_actual
knn = KNeighborsClassifier(k_actual)
knn.fit(X_train,y_train) # pass the variables X values and expected result y from model
training data
knn.score(X_val,y_val)
y_KNN_pred = knn.predict(X_val) # pass the validation X data and get the predictions
```

Performance Parameters

```
# imports
from sklearn.metrics import accuracy_score,confusion_matrix
from sklearn.metrics import classification_report
from sklearn import metrics

cnf_matrix = metrics.confusion_matrix(y_val, y_KNN_pred) # sending actual and predicted
values to get result
accuracy_score(y_val, y_KNN_pred))
classification_report(y_val, y_KNN_pred)
```

⁶ <https://realpython.com/knn-python/>

Appendix C: Calibration procedure

When a spectrometer collects data, it needs calibration with standard reference. The procedure for calibration is similar for reflectance/transmission type.

Lab Step up using Avantes spectrometer.

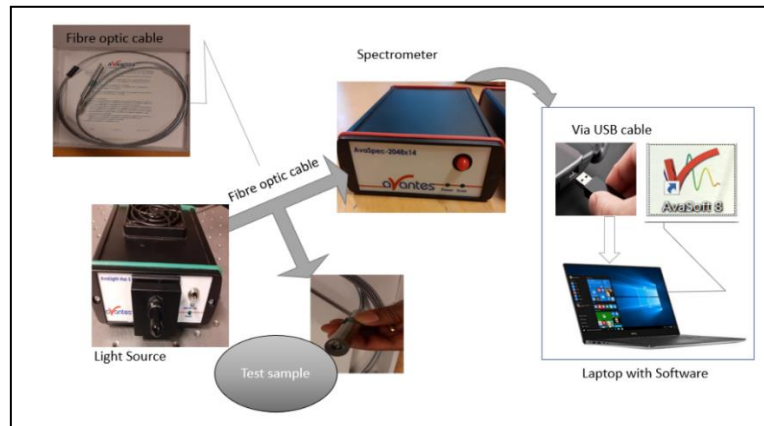


Figure C. 1 Block diagram for Reflectance measurement

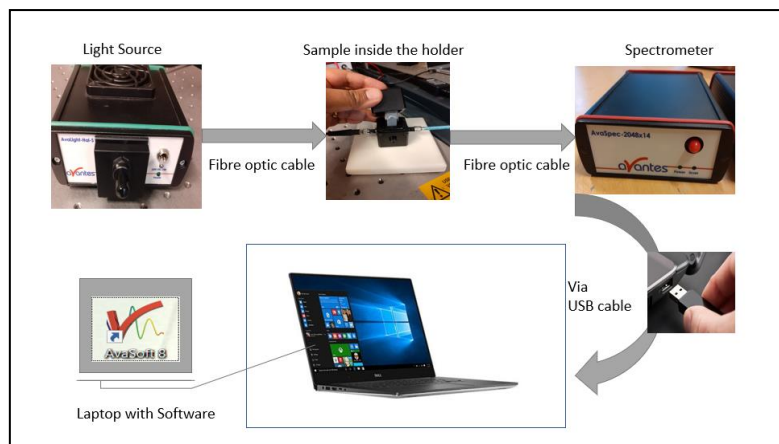


Figure C. 2 Block Diagram for transmission measurement

The device arrangement for reflectance measurements is in figure C.1, while figure C.2 is for transmission. Use a smooth white reflecting surface to calibrate the former and an empty cuvette holder for later. The remaining steps for calibration are the same for both types. Figure A.3 shows how to place the sample for the transmission type of measurement.

Precautions: While using Avantes light source, ensure to turn on the source for 15 minutes. It is the warm-up time for the device.

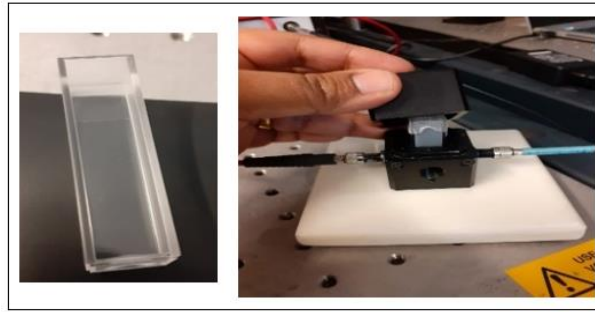


Figure C. 3 Test Sample for measurement in transmission type

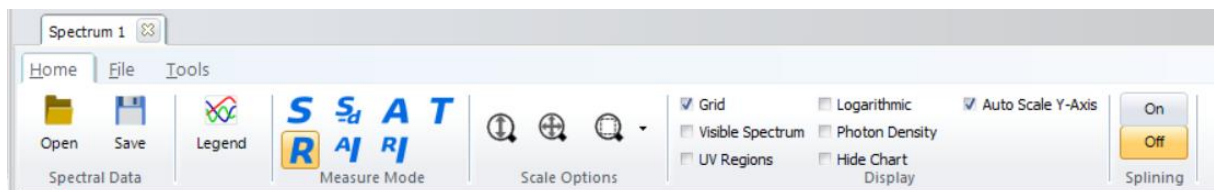






Figure C. 4 AVASOFT GUI interface

Calibration & data collection procedure measurement using AVASOFT.

- Create a new folder to save the experiment set.
- Go to File and click new experiment.
- Refer to figure A.4 with AVASOFT GUI interface for the tabs. Back on the main page, Click the S-icon.
- Place the spectrometer.
- Click the auto integration icon . Ensure to get a curve plot (flat graph means saturations).
- Once the curve is inverted U curve, take the reference reading by clicking the icon  while placing the cylindrical end on the reference surface. The tab turns green and displays a confirmation message on the saved reference.
- Then close the shutter in the light source. Please wait for a moment and then take the dark reading by clicking the tab next to it on the left side . Message on saving dark reference indicates it is complete. After that, the shutter (light is still in ON state).
- Click the R-icon  that indicates the Reflectance Reading. Take the reading of the same reference Surface. It will be around 100 % reflectance. Click the save icon and save the reference if we get such a reading.

- Now place the cylindrical end of the probe on the actual surface whose reflectance measurement is collected.

Changes in transmission measurement

- To take the reference Setting, place an empty cuvette in the cuvette holder and do the reference measurement by taking the light reference (with the shutter open) and dark reference (shutter closed) using an empty cuvette.
- Then place the cuvette with the prepared Gel/solution. Then take an actual reading by clicking/the icon.